Organic geochemistry of the early Toarcian oceanic anoxic event in Hawsker Bottoms, Yorkshire, England

K. L. French[a*], J. Sepúlveda[b], J. Trabucho-Alexandre[c], D. R. Gröcke[c], R. E. Summons[b]

[a] Joint Program in Chemical Oceanography; Massachusetts Institute of Technology and Woods Hole Oceanographic Institution, Cambridge, MA 02139, United States

[b] Department of Earth, Atmospheric, and Planetary Sciences; Massachusetts Institute of Technology, Cambridge, MA 02139, United States

[c] Department of Earth Sciences, University of Durham, Durham, DH1 3LE, UK

*Corresponding author:

E-mail address: klfrench@mit.edu (K. L. French)

Tel: +01 617-324-3953

Abstract

A comprehensive organic geochemical investigation of the Hawsker Bottoms outcrop section in Yorkshire, England has provided new insights about environmental conditions leading into and during the Toarcian oceanic anoxic event (T-OAE; ~183 Ma). Rock-Eval and molecular analyses demonstrate that the section is uniformly within the early oil window. Hydrogen index (HI), organic petrography, polycyclic aromatic hydrocarbon (PAH) distributions, and tricyclic terpane ratios mark a shift to a lower relative abundance of terrigenous organic matter supplied to the sampling locality during the onset of the T-OAE and across a lithological transition. Unlike other ancient intervals of anoxia and extinction, biomarker indices of planktonic community structure do not display major changes or anomalous values. Depositional environment and redox indicators support a shift towards more reducing conditions in the sediment porewaters and the development of a seasonally stratified water column during the T-OAE. In addition to carotenoid biomarkers for green sulfur bacteria (GSB), we report the first occurrence of okenane, a marker of purple sulfur bacteria (PSB), in marine samples younger than ~1.64 Ga. Based on modern observations, a planktonic source of okenane's precursor, okenone, would require extremely shallow photic zone euxinia (PZE) and a highly restricted depositional environment. However, due to coastal vertical mixing, the lack of planktonic okenone production in modern marine sulfidic environments, and building evidence of okenone production in mat-dwelling Chromatiaceae, we propose a sedimentary source of okenone as an alternative. Lastly, we report the first parallel compound-specific $\delta^{13}C$ record in marine- and terrestrial-derived biomarkers across the T-OAE. The $\delta^{13}C$ records of short-chain *n*-alkanes, acyclic isoprenoids, and long-chain *n*-

alkanes all encode negative carbon isotope excursions (CIEs), and together, they support an injection of isotopically light carbon that impacted both the atmospheric and marine carbon reservoirs. To date, molecular $\delta^{13}C$ records of the T-OAE display a negative CIE that is smaller in magnitude compared to the bulk organic $\delta^{13}C$ excursion. Although multiple mechanisms could explain this observation, our molecular, petrographic, and Rock-Eval data suggest that variable mixing of terrigenous and marine organic matter is an important factor affecting the bulk organic $\delta^{13}C$ records of the T-OAE.

Keywords: Toarcian oceanic anoxic event; lipid biomarkers; okenane; photic zone euxinia, stable carbon isotopes; Hawsker Bottoms

1. Introduction

Several transient episodes of enhanced deposition and preservation of organic-rich sediments punctuated the Mesozoic Era. A combination of factors may have caused these intervals, known as oceanic anoxic events (OAEs), including greenhouse conditions and enhanced marine productivity (e.g. Schlanger and Jenkyns, 1976; Jenkyns, 1980; 1988; 2010; Trabucho-Alexandre et al., 2010). The first Mesozoic OAE was the Early Jurassic Toarcian OAE (T-OAE; ~183 Ma), which was associated with elevated extinction rates, enhanced weathering rates, warm temperatures, ocean acidification, and a negative carbon isotope excursion (CIE) (Hesselbo et al., 2000; Cohen et al., 2004; Bambach, 2006; Hesselbo et al., 2007; Jenkyns, 2010; Kiessling and Simpson, 2011). The duration of the T-OAE is not precisely known but may have lasted on the order of several hundred thousand years (Kemp et al., 2005; Suan et al., 2008; Kemp et al., 2011). The Karoo and Ferrar igneous provinces, which erupted at 183 ± 1 Ma, may have coincided with the Pliensbachian-Toarcian extinction (Pálfy and Smith, 2000; Courtillot and Renne, 2003). However, better radiometric dating of the volcanism and OAE are required to confidently link these two events. Although multiple mechanisms have been proposed to account for the Toarcian negative CIE, including methane hydrate dissociation, upwelling of isotopically light waters, thermogenic release of methane, and biomass burning (Hesselbo et al., 2000; Schouten et al., 2000; McElwain et al., 2005; van de Schootbrugge et al., 2005; Finkelstein et al., 2006), the source of the isotopically light carbon remains unclear.

The analysis of sedimentary organic matter provides the opportunity to evaluate environmental and ecological responses to carbon cycle perturbations, as well as potentially constraining the perturbation itself. Previous organic geochemical work across the T-OAE has indicated changes in planktonic community structure and redox chemistry, particularly the development of photic zone euxinia (PZE) (e.g. Farrimond et al., 1989; 1994; Schouten et al., 2000; Pancost et al., 2004; Schwark and Frimmel, 2004; Bowden et al., 2006; van Breugel et al., 2006). However, since biomarker records can reflect local responses, additional comprehensive organic geochemical studies from multiple locations are required to build a global perspective of ecological and environmental change associated with the T-OAE. Here, we investigate the temporal variation of lipid biomarkers, Rock-Eval data, organic petrography, and compound-specific carbon isotopes from the Lower Jurassic section at Hawsker Bottoms, Yorkshire, England.

2. Geologic Setting and Site Description of Hawsker Bottoms, Yorkshire, England

A well-studied section of the Toarcian OAE is located on the Yorkshire coast in northern England. We analyzed sample splits spanning 14 m of an organic-rich, lower Jurassic outcrop section in the Cleveland Basin at Hawsker Bottoms previously studied by Hesselbo et al. (2000). The lithology is dominated by black shales containing discrete levels of calcite concretions and constitutes the Jet Rock *sensu stricto* (Hesselbo and Jenkyns, 1995). The sections around Hawsker Bottoms have been used for defining the ammonite biostratigraphy of the Toarcian (Howarth, 1992).

93 The Early Jurassic paleogeography of the area, although somewhat uncertain, is
94 depicted in published paleogeographic maps (e.g. Bradshaw et al., 1992). The Cleveland
95 Basin of North Yorkshire was part of a system of shallow epicontinental seas and small
96 extensional tectonic basins linked to the Central Graben via the Sole Pit Basin. The
97 region formed part of the broad epicontinental sea that covered much of northwest
98 Europe. Marine sedimentation was initiated during the Late Triassic, and a succession of
99 marine siliciclastic mudstones accumulated during the Early Jurassic.
100 The Grey Shale Member of the Whitby Mudstone Formation consists of
101 bioturbated, silty mudstones with beds of calcareous siderite concretions. The mudstones
102 have thin sharp-based beds, wave ripple, and starved ripple laminations (Wignall et al.,
103 2005; Ghadeer and Macquaker, 2011). Grain size and bioturbation intensity decrease
104 toward the top of the unit, and sediment color darkens. The Jet Rock Member consists of
105 dark, organic matter-rich, fissile mudstones with abundant ammonites and horizons of
106 calcareous nodules. The boundary between these two members of the Whitby Mudstone
107 Formation likely represents an increase in water depth in the basin.
108 The early Toarcian (*D. tenuicostatum* Zone) was a period of major basin
109 subsidence throughout England. Organic matter content fluctuates through the Grey
110 Shales, but increasing levels of organic matter are present from the *D. semicelatum*
111 Subzone to the *C. exaratum* Subzone (*H. falciferum* Zone). Minor shoaling cycles with
112 striped siltstone laminae suggest that water depths were on the order of tens of meters
113 (Powell, 2010). Similarly, sedimentary structures suggest deposition during storms by the
114 effects of waves (Wignall et al., 2005; Ghadeer and Macquaker, 2011). Thus, bottom
115 water conditions were more energetic than is commonly thought, where the water column

116 was likely shallower than 50 m. Consequently, Hawsker Bottoms likely represents an
117 inner continental shelf environment, which physical oceanographers define as the region
118 where turbulence from the surface and bottom boundary layers effectively homogenizes
119 the whole water column (Lentz and Fewings, 2012). Accordingly, inner shelf
120 environments are typically a few meters to tens of meters deep

121 The abundance of ammonites in the shales indicates that the water column was at
122 times oxygenated and favorable to nektonic faunas (Powell, 2010). The abundance of thin
123 beds with tops homogenized by bioturbation suggests that long-term, persistent bottom
124 water anoxia did not occur in the basin (Ghadeer and Macquaker, 2011). Besides
125 deposition as bedload by geostrophic flows and density currents, additional sediment was
126 supplied by suspension settling. Textural analyses have shown that much of the
127 sedimentary organic matter was delivered to the seafloor as fecal pellets, flocs, or other
128 organo-mineralic aggregates (Ghadeer and Macquaker, 2011). The contribution of a
129 biogenic component to rock composition varies, and the differences have been attributed
130 to a changing balance of primary production relative to dilution and length of transport
131 path during deposition (Macquaker and Taylor, 1996; Wignall et al., 2005; Ghadeer and
132 Macquaker, 2011).

133

134 **3. Methods**

135 Powdered rock samples were analyzed by Rock-Eval pyrolysis. The total organic
136 carbon (TOC; %), T_{max} (°C), S_1, and S_2 were determined and used to calculate the
137 hydrogen index (HI) and production index (PI). Kerogen isolates from four samples
138 across the section were mounted onto slides in duplicate and assessed optically under

white light and fluorescent light using a Zeiss research microscope and a Zeiss x 40 Plank-Neofluar objective. A Zeiss Axioskop, Axio Image D1, and a Zeiss 18 filter set were used to take photomicrographs and fluorescence images.

Powdered samples (~ 5 g) were extracted using a Dionex ASE 200 Accelerated Solvent Extractor with a solvent mixture of dichloromethane:methanol 9:1 (v/v). Elemental sulfur was removed from the total lipid extract (TLE). Asphaltenes were separated from the maltene fraction, which was then separated into saturated, aromatic, and polar fractions by silica gel chromatography. The saturated and aromatic fractions were analyzed by gas chromatography-mass spectrometry (GC-MS) and gas chromatography-metastable reaction monitoring-mass spectrometry (GC-MRM-MS). Carbon isotopic measurements of saturated hydrocarbons were made by gas chromatography/combustion/ isotope ratio mass spectrometry (GC-C-IRMS) using a ThermoFinnigan Delta Plus XP coupled to a ThermoFinnigan Trace GC. The mean value of triplicate analyses are reported here in per mil (‰) relative to Vienna Pee Dee belemnite (VPDB), and the standard deviation from the mean value was 0.4‰ or less. A detailed description of methods is included in the supplementary online material (SOM).

4. Results and Discussion

4.1 Rock-Eval analysis

Rock-Eval results provided insight into the thermal maturity and type of organic matter preserved in the Hawsker Bottoms sediments. The TOC percentage (Hesselbo et al., 2000) was plotted for comparison with the HI, PI, and T_{max} (fig. 1). The narrow range of the PI (0.11-0.18) and T_{max} (429-440°C) parameters indicate that thermal maturity is

uniform through the section and at the early stage of oil generation (Peters et al., 2005). Molecular indices of thermal maturity further substantiate this conclusion (see section 4.2).

The HI data reveal that the type of organic matter undergoes a transition that appears to coincide with a lithological transition from medium grey shale to dark grey thin-bedded shale within the limitations of our sampling resolution. The low HI values below -2.5 m are characteristic of type III kerogen, whereas the higher HI values above -3 m are characteristic of type II kerogen (Peters et al., 2005). Type III kerogen is dominated by either terrigenous or highly degraded organic matter, and type II kerogen is typically derived from marine organic matter (Peters et al., 2005).

Published HI values from other T-OAE localities also increase across the initiation of the CIE (Prauss et al., 1991; Schouten et al., 2000; Röhl et al., 2001; Sabatino et al., 2009; Suan et al., 2011). Previous workers have attributed the HI variability to different degrees of organic matter degradation under varying redox conditions (Schouten et al., 2000; Röhl et al., 2001; Sabatino et al., 2009). Alternatively, others have argued that the HI variability represents a shift in the composition of the organic matter (Suan et al., 2011). Petrographic and molecular evidence for the presence of plant-derived material in these sediments (see section 4.3) supports the conclusion that lower HI values at the bottom of the section are due to a larger abundance of terrigenous organic matter relative to marine organic matter.

4.2 Molecular indicators of thermal maturity

184 The thermal history of the section was further assessed according to molecular
185 thermal maturity parameters (fig. 2). The C_{31} hopane 22S/(22S+22R) ratio was constant
186 through the section and exhibited a narrow range between 0.58 and 0.59. A value of
187 ~0.55 represents the endpoint which is reached around the main phase of oil generation
188 (Peters et al., 2005). The C_{30} hopane βα/(βα+αβ) ratio ranged from 0.08 to 0.11, which is
189 close to values indicative of a mature source rock (Peters et al., 2005). The C_{29} sterane
190 ααα 20S/(20S+20R) ratio varied from 0.52 to 0.57, which is comparable to the endpoint
191 value of 0.52-0.55 (Peters et al., 2005). In summary, molecular thermal maturity
192 indicators corroborate the Rock-Eval results, further supporting a uniform thermal
193 maturity within the early window of oil generation.
194 Some biomarker-based thermal maturity parameters can be influenced by
195 additional factors such as source and diagenetic effects (Moldowan et al., 1986; Dahl et
196 al., 1993; Peters et al., 2005; Bennett and Olsen, 2007; French et al., 2012). Indeed, two
197 of the thermal maturity parameters presented in figure 2 exhibit some variation tracking
198 changes in lithology and source input, despite the multiple lines of evidence supporting
199 constant thermal maturity through the section. The Ts/(Ts+Tm) ratio, where Tm is C_{27} 17
200 α -trisnorhopane and Ts is C_{27} 18 α -trisnorhopane, varied from 0.41 to 0.59, whereas the
201 diasterane/sterane ratio of $C_{27\text{-}29}$ compounds ranged from 1.08 to 1.44. Both ratios deviate
202 from a relatively constant pattern in the lower ~2 meters of the section. This pattern is
203 explained by changes in lithology and/or organic matter source input, which is consistent
204 with lower HI values and additional evidence supporting variable terrigenous organic
205 input (see section 4.3).
206

4.3 Biomarker and petrographic evidence of terrigenous organic matter input

A combination of molecular and petrographic analyses was performed to evaluate the relative contribution of terrigenous organic matter through the sampling interval (fig. 3). Previous work has suggested a terrigenous source for C_{19} and C_{20} tricyclic terpanes, which has led to the use of C_{19}/C_{23} and C_{20}/C_{23} tricyclic terpane ratios to identify input of terrigenous organic matter (Noble et al., 1986; Peters et al., 2005). These two ratios display higher values in the lowest part of the section and decrease after the lithological transition at -2.5 meters, indicating relatively greater terrigenous organic matter input in the lowermost part of the sampling interval.

A wide range of PAHs was detected in the Hawsker Bottoms samples, including phenanthrene, fluoranthene, pyrene, benzo[a]anthracene, triphenylene, chrysene, benzo[b]fluoranthene, benzo[k]fluoranthene, benzo[e]pyrene, indeno[c,d]pyrene, dibenzo[a,h]anthracene, benzo[g,h,i]perylene, coronene, and retene. PAHs are a diverse set of compounds with multiple documented sources including products of pyrolysis, combustion, hydrothermal activity, and igneous intrusion as well as direct inputs from algae, fungi, vascular plants, and extraterrestrial organics (Kawka and Simoneit, 1990; George, 1992; Jiang et al., 2000; Sephton et al., 2005; Grice et al., 2007; Marynowski and Simoneit, 2009). PAHs have been used to reconstruct the history of wildfires, higher plant input, and anthropogenic activity, where peri-condensed, unsubstituted PAHs are markers for combustion of organic matter (Hites et al., 1977; Venkatesan and Dahl, 1989; Killops and Massoud, 1992; Kruge et al., 1994; Jiang et al., 1998; Arinobu et al., 1999; Finkelstein et al., 2005; Peters et al., 2005; Marynowski and Simoneit, 2009). Some sedimentary PAHs, such as phenanthrene, chrysene, and triphenylene, are more affected

by diagenesis or additional sources (Jiang et al., 1998; Grice et al., 2007), so they were not included in the total PAH sum plotted in figure 3b. Although the patterns are not identical, enhanced concentrations of total PAH co-occur with elevated C_{19}/C_{23} and C_{20}/C_{23} tricyclic terpane ratios in the bottom 2 meters of the sampling interval. Some PAHS, such as retene, are thought to derive from higher plants, in particular coniferous resin (Wakeham et al., 1980; Ellis et al., 1996; Jiang et al., 1998; Grice et al., 2005; Peters et al., 2005), although algal and bacterial sources have been reported as well (Wen et al., 2000). Retene was detected in all samples, and its concentration was plotted separately as a marker of higher plant input in figure 3c. Retene was more abundant in the lowest interval of the section, which is consistent with the total PAHs, tricyclic terpane ratios, and HI data.

Microscopic analysis of four kerogen samples adds an additional line of evidence supporting stratigraphic variations in kerogen type and organic matter sources. According to the petrographic results, the kerogen is comprised of as much as 80% of terrigenous organic matter in the bottom of the section and about 25-40% in the remainder of the sampling interval (fig. 3d). Since the elemental, molecular, and isotopic composition of organic matter from higher plants is distinct from marine organic matter, HI can reflect the compositional difference of distinct types of organic matter (e.g. Talbot and Livingstone, 1989). Assuming constant HI values for terrigenous and marine organic matter end-members, the percent terrigenous organic matter was estimated through the section using the linear relationship between the percent terrigenous macerals measured by optical microscopy and the corresponding HI (see SOM for more details). Calculated

252 values of $f_{Terr\ OM}$ ranged from 12 to 85%, where the highest values were found in the
253 lowermost part of the section (fig. 3e).

254 The stratigraphic change in the relative supply of terrigenous organic matter ,
255 which is supported by the HI, molecular, and petrographic results, may have been driven
256 by effects related to rising sea level (Hesselbo, 2008; Suan et al., 2011). Considering that
257 increased rates of continental weathering across the T-OAE would have enhanced
258 delivery of terrigenous material (Cohen et al., 2004), the opposite trend recorded in our
259 data might be best explained by progressive remoteness from the coastline on a gently
260 sloping shelf during sea level transgression (e.g. Macquaker et al., 2010). However, sea
261 level related effects might not be the only factor responsible for the changing signal in
262 relative abundance of terrigenous and marine organic matter. For example, enhanced
263 marine export productivity and/or enhanced marine organic matter preservation could
264 have diluted the input of terrigenous organic matter, thereby changing the relative
265 apparent contribution.

266

267 *4.4 Biomarker indicators of source and community structure*

268 Since some compounds or compound classes are associated with a particular
269 biological source, metabolism, or physiology, molecular distributions can be informative
270 about changes in microbial community structure. Unlike other intervals of ocean anoxia
271 associated with mass extinction events (e.g. Xie et al., 2005; Cao et al., 2009), algal- and
272 bacterial-derived biomarkers indicative of community structure did not vary significantly
273 through the CIE (fig. 4). Instead, some biomarker indices that typically reflect
274 community structure were more affected by source input at Hawsker Bottoms.

The regular sterane/17α-hopane ratio is used as an indicator of the relative contributions of eukaryote and bacterial biomass. The regular sterane/hopane ratio was calculated using regular C_{27-29} steranes and 17α C_{29-33} hopanes. The regular sterane/17α-hopane ratio exhibited low values below -2.5 m, whereas it was more elevated (>0.5) and relatively constant in the top 10 m of the section. While this offset could be interpreted as a shift from a bacterially dominated environment in the lower part of the section to a eukaryotic environment above -3 m, it is more likely that a change in the organic matter source input is driving the regular sterane/17α-hopane ratio variability. As well as containing low total steroid abundances, terrigenous organic matter can deliver hopanes derived from soil bacteria, thereby lowering the regular sterane/17α-hopane ratio (Peters et al., 2005; Handley et al., 2010; Sãenz et al., 2011; French et al., 2012).

Similarly, small deviations are found at the bottom of the section for the C_{27}/C_{27-30}, C_{28}/C_{27-30}, and C_{29}/C_{27-30} sterane ratios. These ratios included regular steranes as well as diasteranes and are commonly used as indicators of the relative contribution from red algae biomass, chlorophyll-c algae, and green algae, respectively. However, they can also be affected by the delivery of C_{29} steranes derived from land plants (Moldowan et al., 1985; Peters et al., 2005). Indeed, C_{29} sterane was the dominant sterane in samples from the bottom of the section, where it represented nearly half of the total C_{27-30} steranes. The C_{30}/C_{27-30} sterane ratio, on the other hand, which is an indicator of marine pelagophyte algae, was constant throughout the section and represented only a minor proportion of the total steranes abundance.

The 2α-methylhopane index (2-MHI) has been used as an indicator of cyanobacterial input (Summons et al., 1999), although additional sources were later

298 reported (Rashby et al., 2007). The 3β-methylhopane index (3-MHI) is considered a
299 marker for aerobic proteobacteria, including methanotrophs and acetic acid bacteria
300 (Zundel and Rohmer, 1985; Talbot et al., 2003; Farrimond et al., 2004; Talbot and
301 Farrimond, 2007). The 2-MHI and 3-MHI were invariant, and the 3-MHI was in the
302 range of average Phanerozoic marine values (~1-3%) (Farrimond et al., 2004; Cao et al.,
303 2009). Likewise, the 2-MHI also lacked elevated values. Based on elevated 2-MHI, 3-
304 MHI, and nitrogen isotope anomalies, previous workers have reported an increased
305 contribution of diazotrophic cyanobacteria and methanotrophic bacteria during other
306 OAEs (e.g. Kuypers et al., 2004; Cao et al., 2009; Sepúlveda et al., 2009; Luo et al.,
307 2011). The low and invariant contribution of these microbial groups indicates that
308 environmental conditions suitable for their predominance did not prevail at this locality.
309 Thus, enhanced cyanobacterial diazotrophy may not fully explain the previously reported
310 depleted bulk organic $\delta^{15}N$ at this location during the T-OAE (Jenkyns et al., 2001).
311
312 *4.5 Indicators of redox change and depositional environment*
313 A suite of biomarkers was used to assess changes in water column stratification
314 and redox potential, including the gammacerane index, C_{35} homohopane index (C_{35} HHI),
315 pristane/phytane (Pr/Ph) ratio, and the concentration of aromatic carotenoid derivatives
316 (fig. 5). Although some of these parameters can also be influenced by diagenesis, source
317 input, and thermal maturity, they display patterns consistent with a shift towards more
318 intense reducing conditions at least in the sediment porewaters and potentially in the
319 overlying water column.

Although the biological sources of gammacerane are not fully known (Peters et al., 2005), it is a diagenetic product of tetrahymanol, a compound found in bacteriovorous ciliates thriving at the chemocline of stratified water bodies (ten Haven et al., 1989; Sinninghe Damsté et al., 1995). Thus, the occurrence of gammacerane, expressed as the gammacerane index = *[gammacerane/ (gammacerane + 17α,21β C_{30} hopane)]*100,* has been used to infer changes in water column stratification in ancient environments. Gammacerane was detected in all of the analyzed samples but became more prominent in those deposited during the OAE, starting at the onset of thin-bedded shales.

Elevated abundances of gammacerane during the T-OAE may reflect the development of seasonal water column stratification, possibly due to stronger seasonality and/or deepening of the water column. In contrast, prior to the T-OAE, seasonality may have been weaker, or the water column may have been too shallow to stratify, even during warm months, due to turbulent mixing. The development of seasonal water column stratification at Hawsker Bottoms during the T-OAE would have aided the development of water column oxygen-depletion, particularly during warm and productive months. However, gammacerane enrichments alone do not necessitate water column anoxia, particularly given the association of its precursor, tetrahymanol, with suboxic waters in the modern (Wakeham et al., 2007; 2012).

The C_{35} HHI and Pr/Ph ratio are recorders of depositional redox conditions in sediments. The C_{35} HHI records the degree of preservation of the extended side chain of C_{35} hopanes derived from intact bacteriohopanepolyols (BHPs) (Köster et al., 1997; Peters et al., 2005). Higher C_{35} HHI values are characteristic of oxygen-depleted marine depositional environments. Pristane and phytane in ancient marine rock extracts and oils

343 are largely, but not exclusively, derived from the chlorophyll phytyl side chain from
344 photoautotrophs. Redox conditions influence the diagenetic pathway of the phytyl side
345 chain. Reducing conditions promote the conversion of phytol to phytane, and oxic
346 conditions promote the conversion of phytol to pristane (Didyk et al., 1978; Peters et al.,
347 2005). The C_{35} HHI nearly doubled in samples deposited during the OAE compared to
348 those deposited prior to the event. Values of the Pr/Ph ratio >3 recorded at the bottom of
349 the section are suggestive of deposition of terrigenous organic matter under oxic
350 conditions. The Pr/Ph ratio values near or below 1 during the T-OAE, together with the
351 elevated C_{35} HHI, suggest intensification of reducing conditions in the sediment
352 porewaters during deposition.
353 Biomarkers for anaerobic phototrophic green sulfur bacteria (GSB) have been
354 used to argue for the development of PZE during the T-OAE (Schouten et al., 2000;
355 Pancost et al., 2004; Bowden et al., 2006) and other OAEs (e.g. Cao et al., 2009) based
356 on the physiological requirement of co-occurring reduced sulfur species and light. We
357 detected 2,3,6-aryl isoprenoids, isorenieratane, and chlorobactane in all samples. Unlike
358 previous studies of the T-OAE or any Phanerozoic organic geochemical study of marine
359 samples, trace concentrations of okenane were also identified by GC-MRM-MS in
360 samples above -3 m, whereas it was below detection limit in samples from the lowest 2
361 meters of the section. Okenone, a photosynthetic pigment belonging to the PSB family
362 Chromatiaceae, is the only known precursor of okenane (Brocks and Schaeffer, 2008).
363 All compounds were compared with an authentic carotenoid standard and an extract from
364 the Barney Creek Formation (BCF; fig. 6; Brocks et al., 2005). Normalizations of the C_{40}

365 aromatic carotenoid derivatives against the mass of TOC and TLE reveal a similar pattern
366 of elevated concentrations during the anoxic event compared to the pre-event baseline.
367 In total, all of the organic geochemical redox indicators point towards a shift
368 towards more reducing conditions broadly corresponding with the initiation of the
369 negative CIE. However, sedimentological features, such as starved wave and combined
370 flow ripples, indicate that this area was an energetic, shallow inner shelf environment on
371 the order of tens of meters and probably no deeper than 50 m, where enough oxygen was
372 present in the water column on some timescale to sustain nektonic fauna, including
373 ammonites, and allow for bioturbation at the sediment-water interface through the OAE
374 (Wignall et al., 2005; Powell, 2010; Ghadeer and Macquaker, 2011). We explore
375 different scenarios to reconcile these apparent opposing lines of evidence.
376 First, the geochemical and sedimentological signals recorded in the rock record
377 are a composite of many processes occurring on different timescales. In the modern
378 ocean, highly productive coastal and continental margin sediments and the overlying
379 water column oscillate between oxic and anoxic conditions over different timescales (e.g.
380 Burdige, 2007). Enhanced productivity and export of organic matter, which are important
381 features of Mesozoic OAEs (e.g. Erba, 2004; Jenkyns, 2010), would have increased the
382 oxygen demand in the water column and sediment porewaters during productive months.
383 During the T-OAE, anoxic conditions may have been restricted to the sediment
384 porewaters during seasons of low productivity, allowing bioturbation to occur when
385 bottom waters were better oxygenated. Conversely, oxygen-deficient waters may have
386 expanded seasonally to the water column during intervals of high productivity and
387 enhanced stratification, as implied by the gammacerane index.

388 Second, the molecular, paleontological, and sedimentary indicators of redox
389 chemistry apply to different parts of the depositional environment, diagenetic pathways,
390 and have different sensitivities along the redox spectrum. With the exception of the GSB
391 and PSB carotenoid markers, the geochemical parameters reported here do not require
392 strict anoxia or euxinia in the water column. The gammacerane index pattern supports the
393 development of seasonal stratification during the OAE, which would have promoted
394 oxygen depletion of the water column. However, the possibility remains that even during
395 intervals of high productivity and stratification, water column oxygen concentrations at
396 this location were depleted but high enough to sustain organisms with physiological
397 oxygen requirements, thereby explaining the fossil and sedimentary evidence.
398 Additionally, the Pr/Ph ratio and C_{35} HHI pertain primarily to sedimentary redox
399 conditions opposed to water column redox structure. Therefore, the occurrence of intact
400 aromatic carotenoid derivatives merits further discussion to assess water column redox
401 chemistry.
402 To date, okenane has only been reported in Paleoproterozoic rock extracts and
403 lacustrine Cenozoic extracts (Brocks et al., 2005; Zhang et al., 2011). Given the
404 atmospheric pO_2 during the Mesozoic was near present atmospheric levels (Berner,
405 2006), its detection in marine samples of this age requires careful interpretation. The PSB
406 family Chromatiaceae blooms in a range of anoxic environments with light and reduced
407 sulfur species, including stratified lakes, fjords, coastal lagoons, estuaries, and coastal
408 microbial mats, but not all Chromatiaceae produce okenone (Brocks and Schaeffer, 2008
409 and references therein). Okenone-producing planktonic Chromatiaceae dwell in water
410 columns where the chemocline is above 25 m and in 75% of the reported cases less than

411 12 m (Brocks and Schaeffer, 2008). Notably, all of the modern chemocline depth
412 observations for okenone production are based on stratified lake systems. Thus, the lack
413 of okenone in modern marine sulfidic environments presents a "no analogue problem" for
414 ancient marine samples containing okenane that were deposited under atmospheric pO_2
415 close to modern levels.

416 Transient free sulfide has been reported in the water column of intense upwelling
417 zones, including the Arabian Sea, Namibian coast, and the Peruvian coast (e.g Dugdale et
418 al., 1977; Brüchert et al., 2003; Naqvi et al., 2006; Schunck et al., 2013). However, these
419 episodes are typically short lived. In contrast, sulfidic waters persist in some restricted
420 marine basins and fjords, including the Black Sea, Cariaco Basin, Saanich Inlet, and the
421 Framvaren and Effingham Fjords. However, these two types of marine environments
422 (non-restricted, transiently sulfidic and restricted, permanently sulfidic) fail to represent
423 suitable modern analogues for Hawsker Bottoms on several counts. Isorenieratene has
424 been measured in the water column and sediments of some restricted marine basins,
425 particularly fjords and the Black Sea (e.g. Sinninghe Damsté and Schouten, 2006), but
426 GSB carotenoids have not been detected in transiently sulfidic upwelling systems.
427 Furthermore, okenone has not been reported in the water column or sediments of any
428 modern marine transiently or permanently sulfidic environment, with the exception of the
429 upper sediments of Kyllaren fjord, a small, highly restricted basin (Smittenberg et al.,
430 2004; Sinninghe Damsté and Schouten, 2006). Like okenone, modern planktonic marine
431 occurrences of chlorobactene are also limited to semi-enclosed water masses that are not
432 representative of fully marine conditions (e.g. Naeher et al. 2012). Interestingly, multiple
433 emerging lines of evidence suggest the occurrence of a "cryptic sulfur cycle" in some

434 OMZs, with a potential role for photosynthetic sulfide oxidation (Canfield et al., 2010;
435 Stewart et al., 2012). However, the presence of GSB and/or PSB and their respective
436 carotenoids have yet to be reported in modern OMZs.

437 Furthermore, the physical oceanographic processes determining the degree of
438 vertical mixing, hence stratification and redox gradient stability, are markedly different
439 between inner shelf environments and sulfidic, silled basins, which are highly restricted
440 and in many classic modern examples, are an order of magnitude or more deeper than
441 estimated paleodepths of Hawsker Bottoms. Although the water column at Hawsker
442 Bottoms became deeper with the sea level transgression across the T-OAE, the
443 depositional environment remained relatively shallow because of its location on a gently
444 sloping shelf (e.g. Macquaker et al., 2010). Consequently, turbulent mixing at the surface
445 and bottom boundary layers would have prevented a stable sulfidic chemocline from
446 developing. On the other hand, considering the limited occurrence of planktonically
447 produced okenone in modern lakes, a planktonic source of okenone at Hawsker Bottoms
448 would imply that, rather than an inner sheld environment, Hawsker Bottoms was a highly
449 restricted coastal basin not reflective of fully marine conditions.

450 Alternatively, we argue that okenane at Hawsker Bottoms was likely derived from
451 benthic microbial mats based on the lack of modern analogues of okenone-production in
452 marine sulfidic environments, the dynamics of inner shelf physical mixing, and building
453 evidence of okenone-producing, mat-dwelling Chromatiaceae (e.g. Caumette et al., 1991;
454 Airs et al., 2001; Caumette et al., 2004; Meyer et al., 2011). Furthermore, planktonic
455 Chlorobiaceae are not the exclusive source of isorenieratene and chlorobactene. Previous
456 work has documented additional non-planktonic GSB sources of isorenieratene and

chlorobactene, including microbial mats (e.g.Wahlund et al., 1991; Brocks and Summons, 2003; Beatty et al., 2005; Bühring et al., 2011). Although a mixed planktonic and mat origin of the carotenoids cannot be ruled out, it is more likely that the GSB and PSB carotenoids detected in Hawsker Bottoms samples share a source. Previous studies of sedimentary structures in the Toarcian shales of Yorkshire have attributed wavy laminations to microbial mats (O'Brien, 1990), thereby further supporting a sedimentary origin of GSB and PSB carotenoid derivatives detected in Hawsker Bottoms samples. Similar wavy laminated fabrics have been reported in coeval shales in northern European T-OAE sections (Trabucho-Alexandre et al., 2012). Unfortunately, a sedimentary source of the GSB and PSB carotenoid derivatives offers little information about water column redox chemistry. However, this interpretation does not preclude the development of a suboxic, anoxic, or euxinic water column in this region on some timescale during the T-OAE. Instead, additional inorganic geochemical data is required to better assess the water column redox conditions and degree of basin restriction (Algeo and Tribovillard, 2009).

4.6 Compound specific stable carbon isotopic data

A limited number of compound specific $\delta^{13}C$ records of the T-OAE are currently available in the literature. Here, we report the first long-chain *n*-alkane $\delta^{13}C$ records of the T-OAE. Compound specific $\delta^{13}C$ analyses of marine- and terrestrial-derived lipids reveal a shift towards lighter $\delta^{13}C$ values (fig. 7). Short-chain *n*-alkanes, as well as pristane and phytane are typically used as marine indicators, whereas long-chain *n*-alkanes primarily reflect terrigenous sources. The *n*-C_{17}, *n*-C_{18}, and *n*-C_{19} alkanes displayed a negative excursion of ~2–3‰, which is consistent with the ~2–4‰ negative

480 excursions documented in the partial n-C_{16-20} alkane records from the Toarcian
481 Posidonienschiefer in southwest Germany (Schouten et al., 2000). Pristane and phytane
482 encode a muted excursion (~1.5–2‰) compared to short-chain alkane records, and they
483 also have smaller CIE magnitudes compared to the pristane and phytane isotopic records
484 from the Toarcian Paris Basin and the Posidonienschiefer (~3–4‰) (Schouten et al.,
485 2000; van Breugel et al., 2006). On the other hand, long-chain *n*-alkanes (*n*-C_{27}, *n*-C_{28},
486 and *n*-C_{29}), which are primarily but not exclusively derived from epicuticular waxes of
487 vascular plants (Eglinton and Hamilton, 1967), display the largest compound specific
488 negative CIE (~4–5‰). The molecular isotopic records appear to register the initiation of
489 the negative CIE earlier than in the bulk organic record, and within the CIE, the
490 compound-specific $\delta^{13}C$ values remain fairly stable while the bulk curve becomes
491 gradually depleted. However, these features could be due to sampling resolution
492 differences. Higher resolution molecular isotopic records are required to better address
493 the timing and structure of the isotopic excursion recorded in different carbon reservoirs.
494 The absolute magnitude of the bulk organic CIE (~5–7‰) is larger than the CIEs
495 recorded in the molecular records from Yorkshire (this study; ~1.5–5‰), the Paris Basin
496 (~3‰; van Breugel et al., 2006), and the Posidonienschiefer (~2–4‰; Schouten et al.,
497 2000). Identifying the reason behind the CIE magnitude offsets is critical for placing
498 bounds on the magnitude of isotopically light carbon added into the system. Bulk organic
499 matter is comprised of an array of molecularly and isotopically heterogeneous
500 constituents. In addition to environmental perturbations, organic matter source mixing
501 can contribute to bulk organic $\delta^{13}C$ excursions (e.g. Pancost et al., 1999). The comparison
502 of short- and long-chain *n*-alkane isotopic compositions demonstrates that, unlike the

503 modern, terrigenous organic matter is isotopically heavier than marine organic matter
504 during the Toarcian (fig. 7), which is consistent with previous Toarcian studies (Vetö et
505 al., 1997; Schouten et al., 2000). Multiple lines of evidence presented in section 4.3
506 highlight a significant transition in the terrigenous organic matter input at Hawsker
507 Bottoms. Indeed, the bottom 2 meters of the study interval are dominated by terrigenous
508 organic matter and are isotopically heavier than the overlying interval that is dominated
509 by marine organic matter. Therefore, an undetermined component of the bulk organic
510 CIE magnitude may be attributed to source mixing effects.

511 Additional factors could also contribute to the difference in magnitudes between
512 bulk and molecular CIEs. For instance, it is possible that the full CIE was not captured in
513 the molecular isotopic records due to a lower sampling resolution compared to the bulk
514 organic $\delta^{13}C$ records. Alternatively, water availability can modulate the magnitude of the
515 CIE recorded in vascular leaf waxes, as has been discussed for the Paleocene Eocene
516 Thermal Maximum (PETM; e.g. Schouten et al., 2007; Smith et al., 2007), but unlike the
517 PETM, the ratio of angiosperms and conifers would not account for the *n*-alkane and bulk
518 organic CIE magnitude offset because the rise of angiosperms postdates the Early
519 Jurassic (e.g. Heimhofer et al., 2005). Additionally, thermal maturation could influence
520 the $\delta^{13}C$ of individual compounds, which become isotopically heavier with increasing
521 thermal maturity (Clayton, 1991; Clayton and Bjorøy, 1994; Tang et al., 2005).

522 Nevertheless, while multiple mechanisms may account for the difference between
523 molecular and bulk organic CIE magnitudes, it is significant that a negative CIE is
524 recorded in both marine- and terrestrial-derived lipids, albeit to different degrees. The
525 parallel isotopic change in marine and terrestrial carbon pools recorded at Hawsker

Bottoms further supports previous studies suggesting that the T-OAE was a global carbon cycle perturbation where isotopically light carbon entered the atmospheric, terrigenous, and marine carbon reservoirs (Hesselbo et al., 2000; 2007; Al-Suwaidi et al., 2010; Caruthers et al., 2011; Gröcke et al., 2011). Multiple sources of isotopically light carbon have been proposed, including methane hydrate dissociation, regional upwelling of isotopically light waters in stratified epicontinental seas, thermogenic release of methane from organic-rich strata in contact with dykes, biomass burning, or a combination of these mechanisms (Hesselbo et al., 2000; Schouten et al., 2000; McElwain et al., 2005; van de Schootbrugge et al., 2005; Finkelstein et al., 2006).

Although our study does not provide evidence in support of a specific forcing mechanism, it allows us to narrow down potential mechanisms. A deep-water source of isotopically light carbon is unlikely because of the CIE observed in land plant biomarkers. The lack of evidence for bacterial methanotrophy in our section suggests that methane hydrate dissociation did not supply appreciable methane to the sampling locality. The organic matter source transition complicates the interpretation of PAH abundances as tracers of biomass burning, so a different sampling locality without an organic matter source transition should be studied to test the biomass burning mechanism using PAHs. A cascade of mechanisms rather than a single mechanism likely initiated the T-OAE. However, our results indicate that the influence of source mixing on the bulk organic $\delta^{13}C$ has been previously underestimated and could have potentially affected other bulk isotopic systematics such as nitrogen. Therefore, previous estimates regarding the magnitude of this global perturbation of the carbon cycle should be revisited.

5. Conclusions

We use a multiproxy approach based on bulk geochemistry, lipid biomarkers, and compound-specific stable isotopes to elucidate environmental and ecological changes associated with the T-OAE at Hawsker Bottoms in Yorkshire, England. Molecular indicators and Rock-Eval results suggest that thermal maturity is uniformly in the early oil generation window throughout the sampling interval. The HI data, organic petrography, PAH distribution, and tricyclic terpane ratios indicate a transition in the relative input of terrigenous vs. marine organic matter across a lithological transition. The shift to lower relative abundance of terrigenous organic matter was likely a result of sea level related effects such as coastal proximity, changes in marine organic matter preservation, and/or dilution effects from increased marine productivity.

Organic geochemical redox and depositional environment indicators point towards an overall shift towards more reducing conditions in sediment porewaters and the development of seasonal stratification during the OAE. Previous sedimentological observations require that the water column was not completely anoxic throughout the entire T-OAE, which may seem contradictory at first to the detection of GSB and PSB carotenoids. However, here we present the first occurrence of okenane, a carotenoid marker of PSB, in marine samples younger than the Paleoproterozoic (1.64 Ga). This unexpected finding challenges the interpretation of GSB and PSB carotenoids as markers of PZE in the context of Hawsker Bottoms due to inner shelf vertical mixing, the lack of modern analogues of okenone-production in marine sulfidic environments, and the emerging evidence of okenone-producing mat-dwelling Chromatiaceae. Therefore, in combination with previous reports of microbial wavy lamination in Toarcian shales of

572 Yorkshire and coeval shales in northern Europe, we argue that okenane, and potentially
573 chlorobactane and isorenieratane, was most likely mat-derived at Hawsker Bottoms.
574 The compound-specific $\delta^{13}C$ records of short-chain *n*-alkanes, acyclic
575 isoprenoids, and long-chain *n*-alkanes support a carbon cycle perturbation that affected
576 both the atmospheric and marine systems, which precludes the recycling of isotopically
577 light CO_2 from anoxic waters as the sole mechanism responsible for the T-OAE negative
578 CIE. Notably, compound specific $\delta^{13}C$ records of the T-OAE, including the new data
579 presented here from Yorkshire and previous molecular data from the Paris Basin and the
580 Posidonienschiefer, encode negative CIEs that are smaller in magnitude compared to bulk
581 organic $\delta^{13}C$ records. Many mechanisms could contribute to this observation, particularly
582 variable mixing of terrigenous and marine organic matter, which is supported by the
583 multiple lines of evidence for a transition in organic matter source. Identifying the
584 mechanisms behind the CIE magnitude offsets is important for estimating the magnitude
585 of isotopically light carbon injected into the surface carbon reservoirs.
586
587 Acknowledgements
588 We thank Alison Cohen and Emma Grosjean for their contributions to the early
589 stages of this study, Lorraine Eglinton for petrographic analysis, Carolyn Colonero for
590 laboratory assistance, and three anonymous reviewers for valuable comments that
591 improved this work. Funding support for work at MIT was provided by grants from the
592 NASA Astrobiology Institute and the NASA Exobiology Program to RES and an NSF
593 graduate fellowship to KLF. This project was partly funded by a NSERC Discovery

Grant (# 288321) and NERC Standard Grant (NE/H021868/1) to DRG. JTA is funded by the NERC Standard Grant (NE/H021868/1) to DRG.

Figure Captions:

Fig. 1. Rock-Eval Analysis. A) Total organic carbon (TOC; %) (Hesselbo et al., 2000); B) Hydrogen index (HI; mg HC/g TOC); C) Production index (PI); D) T_{max} (°C).

Fig. 2. Molecular Indicators of Thermal Maturity. A) The C_{31} hopane 22S/(22S+22R) ratio; B) C_{30} hopane βα/(βα+αβ) ratio; C) C_{29} sterane ααα 20S/(20S+20R) ratio; D) Ts/(Ts+Tm) ratio; E) diasteranes/steranes ratio. Note the lack of variation in A, B and C across the section compared to the minor variations exhibited by D and E due to changes in source input and/or lithology.

Fig 3. Terrigenous Organic Matter Indicators. A) Ratios of C_{19}/C_{23} and C_{20}/C_{23} tricyclic terpanes; B) total concentration of PAHs normalized by TOC and TLE; C) concentration of retene normalized by TOC and TLE; D) measured contribution of terrigenous organic matter (OM) by petrographic analysis; E) calculated percentage of terrigenous organic matter ($f_{Terr\ OM}$) based on linear regression ($f_{Terr\ OM}$ (%) = -0.279 * HI + 136; R^2=0.90) of petrographic measurements of terrigenous organic matter (Fig. 3D) and HI (Fig. 1B).

Fig. 4. Source and Community Indicators. A) The ratio of regular steranes/17α-hopanes; B) $C_{27}/C_{27\text{-}30}$ steranes; C) $C_{28}/C_{27\text{-}30}$ steranes; D) $C_{29}/C_{27\text{-}30}$ steranes; E) 2α-methylhopane and 3β-methylhopane indices.

Fig. 5. Redox and Depositional Environmental Indicators. A) Gammacerane index; B) C_{35} homohopane index (C_{35}HHI); C) pristane/phytane (Pr/Ph) ratio; D) concentration of isorenieratane; E) concentration of chlorobactane; F) concentration of okenane. The concentrations of C_{40} carotenoids are semi-quantitative and were normalized against TOC and TLE.

Fig. 6 Gas chromatography - metastable reaction monitoring - mass spectrometry (GC-MRM-MS) chromatogram for the identification of aromatic carotenoid derivatives. MRM chromatograms displaying the 554→134 transition characteristic for chlorobactane and okenane in an authentic standard of combined C_{40} carotenoids (A) and in sample ENR004 at 5.98 m (C). Plots B and D are MRM chromatograms displaying the 546→134 MRM transition characteristic of isorenieratane, renieratane, and renierapurpurane in an authentic standard of combined C_{40} carotenoid (B) and in sample ENR004 (D). Compound abbreviations were used for labels: chlorobactane (Ch); okenane (Ok); isorenieratane (Iso); renieratane (Ren); renierapurpurane (Rpurp).

635 **Fig. 7 Carbon Isotopic records**. A) Previously reported $\delta^{13}C_{org}$ from Hawsker Bottoms
636 (Hesselbo et al., 2000; Kemp et al., 2005); B) $\delta^{13}C$ of n-C_{17-19} short-chain n-alkanes; C)
637 $\delta^{13}C$ of pristane and phytane; D) $\delta^{13}C$ of n-C_{27-29} long-chain n-alkanes. Note the different
638 x-axis scales.
639

640 References
641
642 Airs, R.L., Atkinson, J.E., Keely, B.J., 2001. Development and application of a high
643 resolution liquid chromatographic method for the analysis of complex pigment
644 distributions. J. Chromatogr. A 917, 167–177.
645 Algeo, T. J., Tribovillard, N., 2009. Environmental analysis of paleoceanographic
646 systems based on molybdenum-uranium covariation. Chem. Geol. 268, 211-225.
647 Al-Suwaidi, A.H., Angelozzi, G.N., Baudin, F., Damborenea, S.E., Hesselbo, S.P.,
648 Jenkyns, H.C., Mancenido, M.O., Riccardi, A.C., 2010. First record of the Early
649 Toarcian Oceanic Anoxic Event from the Southern Hemisphere, Neuquén Basin,
650 Argentina. J. Geol. Soc. (London) 167, 633–636.
651 Arinobu, T., Ishiwatari, R., Kaiho, K., Lamolda, M.A., 1999. Spike of pyrosynthetic
652 polycyclic aromatic hydrocarbons associated with an abrupt decrease in $\delta^{13}C$ of a
653 terrestrial biomarker at the Cretaceous-Tertiary boundary at Caravaca, Spain.
654 Geology 27, 723–726.
655 Bambach, R.K., 2006. Phanerozoic biodiversity mass extinctions. Annu. Rev. Earth
656 Planet. Sci. 34, 127–155.
657 Beatty, J., Overmann, J., Lince, M., Manske, A., Lang, A., Blankenship, R., Van Dover,
658 C., Martinson, T., Plumley, F., 2005. An obligately photosynthetic bacterial anaerobe
659 from a deep-sea hydrothermal vent. Proc. Natl. Acad. Sci. U.S.A 102, 9306–9310.
660 Bennett, B., Olsen, S., 2007. The influence of source depositional conditions on the
661 hydrocarbon and nitrogen compounds in petroleum from central Montana, USA. Org.
662 Geochem. 38, 935–956.
663 Berner, R., 2006. GEOCARBSULF: A combined model for Phanerozoic atmospheric O_2
664 and CO_2. Geochim. Cosmochim. Acta 70, 5653–5664.
665 Bowden, S.A., Farrimond, P., Snape, C.E., Love, G.D., 2006. Compositional differences
666 in biomarker constituents of the hydrocarbon, resin, asphaltene and kerogen
667 fractions: An example from the Jet Rock (Yorkshire, UK). Org. Geochem. 37, 369–
668 383.
669 Bradshaw, M J, J C W Cope, D W Cripps, D T Donovan, M K Howarth, P F Rawson, I
670 M West, and W A Wimbledon. 1992. “Jurassic.” Geol. Soc., London, Memoirs 13,
671 107–129.
672 Brocks, J., Love, G., Summons, R., Knoll, A., Logan, G., Bowden, S., 2005. Biomarker
673 evidence for green and purple sulphur bacteria in a stratified Palaeoproterozoic sea.
674 Nature 437, 866–870.
675 Brocks, J., Schaeffer, P., 2008. Okenane, a biomarker for purple sulfur bacteria
676 (Chromatiaceae), and other new carotenoid derivatives from the 1640 Ma Barney
677 Creek Formation. Geochim. Cosmochim. Acta 72, 1396–1414.
678 Brocks, J.J., Summons, R.E., 2003. Sedimentary hydrocarbons, biomarkers for early life.
679 In: Treatise on Geochemistry, (Elsevier-Pergamon, Oxford). Chpt. 8.03, pp. 63–115.
680 Brüchert, V., Jørgensen, B.B., Neumann, K., Riechmann, D., Schlösser, M., Schulz, H.,
681 2003. Regulation of bacterial sulfate reduction and hydrogen sulfide fluxes in the
682 central Namibian coastal upwelling zone. Geochim. Cosmochim. Acta 67, 4505–
683 4518.
684 Burdige, D., 2007. Preservation of organic matter in marine sediments: controls,
685 mechanisms, and an imbalance in sediment organic carbon budgets? Chem. Rev.

686 107, 467–485.
687 Bühring, S., Sievert, S., Jonkers, H., Ertefai, T., Elshahed, M., Krumholz, L., Hinrichs, K.
688 -U., 2011. Insights into chemotaxonomic composition and carbon cycling of
689 phototrophic communities in an artesian sulfur-rich spring (Zodletone, Oklahoma,
690 USA), a possible analog for ancient microbial mat systems. Geobiol. 9, 166–179.
691 Canfield, D.E., Stewart, F.J., Thamdrup, B., De Brabandere, L., Dalsgaard, T., Delong,
692 E.F., Revsbech, N.P., Ulloa, O., 2010. A Cryptic Sulfur Cycle in Oxygen-Minimum-
693 Zone Waters off the Chilean Coast. Science 330, 1375–1378.
694 Cao, C., Love, G.D., Hays, L., Wang, W., Shen, S., Summons, R.E., 2009.
695 Biogeochemical evidence for euxinic oceans and ecological disturbance presaging
696 the end-Permian mass extinction event. Earth Planet. Sci. Lett. 281, 188–201.
697 Caruthers, A.H., Gröcke, D.R., Smith, P.L., 2011. The significance of an Early Jurassic
698 (Toarcian) carbon-isotope excursion in Haida Gwaii (Queen Charlotte Islands),
699 British Columbia, Canada. Earth Planet. Sci. Lett. 307, 19–26.
700 Caumette, P., Baulaigue, R., Matheron, R., 1991. *Thiocapsa halophila* sp. nov., a new
701 halophilic phototrophic purple sulfur bacterium. Arch. Microbiol. 155, 170–176.
702 Caumette, P., Guyoneaud, R., Imhoff, J., Süling, J., Gorlenko, V., 2004. *Thiocapsa*
703 *marina* sp. nov., a novel, okenone-containing, purple sulfur bacterium isolated from
704 brackish coastal and marine environments. Int. J. Syst. Evol. Microbiol. 54, 1031–
705 1036.
706 Clayton, C., 1991. Effect of maturity on carbon isotope ratios of oils and condensates.
707 Org. Geochem. 17, 887–899.
708 Clayton, C., Bjorøy, M., 1994. Effect of maturity on $^{13}C/^{12}C$ ratios of individual
709 compounds in North Sea oils. Org. Geochem. 21, 737–750.
710 Cohen, A.S., Coe, A.L., Harding, S.M., Schwark, L., 2004. Osmium isotope evidence for
711 the regulation of atmospheric CO_2 by continental weathering. Geology 32, 157–160.
712 Courtillot, V.E., Renne, P.R., 2003. On the ages of flood basalt events. C. R. Geoscience
713 335, 113–140.
714 Dahl, J., Moldowan, J., M., Sundararaman, P., 1993. Relationship of biomarker
715 distribution to depositional environment: Phosphoria Formation, Montana, USA.
716 Org. Geochem. 20, 1001–1017.
717 Didyk, B., Simoneit, B., Brassell, S., Eglinton, G., 1978. Organic geochemical indicators
718 of palaeoenvironmental conditions of sedimentation. Nature 272, 216-222.
719 Dugdale, R., Goering, J., Barber, R., Smith, R., Packard, T., 1977. Denitrification and
720 hydrogen sulfide in the Peru upwelling region during 1976. Deep-Sea Res. 24, 601–
721 608.
722 Eglinton, G., Hamilton, R., 1967. Leaf epicutular waxes. Science. 156, 1322-1335.
723 Ellis, L., Singh, R.K., Alexander, R., Kagi, R.I., 1996. Formation of isohexyl
724 alkylaromatic hydrocarbons from aromatization-rearrangement of terpenoids in the
725 sedimentary environment: A new class of biomarker. Geochim. Cosmochim. Acta
726 60, 4747–4763.
727 Erba, E., 2004. Calcareous nannofossils and Mesozoic oceanic anoxic events. Mar.
728 Micropaleontol. 52, 85–106.
729 Farrimond, P., Eglinton, G., Brassell, S., Jenkyns, H., 1989. Toarcian anoxic event in
730 Europe: an organic geochemical study. Mar. Petrol. Geol. 6, 136–147.
731 Farrimond, P., Stoddart, D., Jenkyns, H., 1994. An Organic Geochemical Profile of the

732 Toarcian Anoxic Event in Northern Italy. Chem. Geol. 111, 17–33.
733 Farrimond, P., Talbot, H.M., Watson, D.F., Schulz, L.K., Wilhelms, A., 2004.
734 Methylhopanoids: Molecular indicators of ancient bacteria and a petroleum
735 correlation tool. Geochim. Cosmochim. Acta 68, 3873–3882.
736 Finkelstein, D.B., Pratt, L.M., Brassell, S.C., 2006. Can biomass burning produce a
737 globally significant carbon-isotope excursion in the sedimentary record? Earth
738 Planet. Sci. Lett. 250, 501–510.
739 Finkelstein, D.B., Pratt, L.M., Curtin, T.M., Brassell, S.C., 2005. Wildfires and seasonal
740 aridity recorded in Late Cretaceous strata from south-eastern Arizona, USA.
741 Sedimentology 52, 587–599.
742 French, K.L., Tosca, N.J., Cao, C., Summons, R.E., 2012. Diagenetic and detrital origin
743 of moretane anomalies through the Permian–Triassic boundary. Geochim.
744 Cosmochim. Acta 84, 104–125.
745 George, S.C., 1992. Effect of igneous intrusion on the organic geochemistry of a siltstone
746 and an oil shale horizon in the Midland Valley of Scotland. Org. Geochem. 18, 705–
747 723.
748 Ghadeer, S.G., Macquaker, J.H.S., 2011. Sediment transport processes in an ancient mud-
749 dominated succession: a comparison of processes operating in marine offshore
750 settings and anoxic basinal environments. J. Geol. Soc. (London) 168, 1121–1132.
751 Grice, K., Backhouse, J., Alexander, R., Marshall, N., Logan, G.A., 2005. Correlating
752 terrestrial signatures from biomarker distributions, $\delta^{13}C$, and palynology in fluvio-
753 deltaic deposits from NW Australia (Triassic–Jurassic). Org. Geochem. 36, 1347–
754 1358.
755 Grice, K., Nabbefeld, B., Maslen, E., 2007. Source and significance of selected
756 polycyclic aromatic hydrocarbons in sediments (Hovea-3 well, Perth Basin, Western
757 Australia) spanning the Permian-Triassic boundary. Org. Geochem. 38, 1795–1803.
758 Gröcke, D., Hori, R., Trabucho-Alexandre, J., Kemp, D., Schwark, L., 2011. An open
759 marine record of the Toarcian oceanic event. Solid Earth 2, 245–257.
760 Handley, L., Talbot, H.M., Cooke, M.P., Anderson, K.E., Wagner, T., 2010.
761 Bacteriohopanepolyols as tracers for continental and marine organic matter supply
762 and phases of enhanced nitrogen cycling on the late Quaternary Congo deep sea fan.
763 Org. Geochem. 41, 910–914.
764 Heimhofer, U., P. A. Hochuli, S. Burla, J. M. L. Dinis, and H. Weissert., 2005. Timing of
765 Early Cretaceous angiosperm diversification and possible links to major
766 paleoenvironmental change. Geology 33, 141-144.
767 Hesselbo, S., 2008. Sequence stratigraphy and inferred relative sea-level change from the
768 onshore British Jurassic. P. Geologist Assoc. 119, 19–34.
769 Hesselbo, S., Jenkyns, H., 1995. A comparison of the Hettangian to Bajocian successions
770 of Dorset and Yorkshire, in: Taylor, P. (Ed.), Field Geology of the British Jurassic.
771 Geological Society of London, pp. 105–150.
772 Hesselbo, S.P., Gröcke, D.R., Jenkyns, H.C., Bjerrum, C.J., Farrimond, P., Morgans Bell,
773 H.S., Green, O.R., 2000. Massive dissociation of gas hydrate during a Jurassic
774 oceanic anoxic event. Nature 406, 392–395.
775 Hesselbo, S.P., Jenkyns, H.C., Duarte, L.V., Oliveira, L.C.V., 2007. Carbon-isotope
776 record of the Early Jurassic (Toarcian) Oceanic Anoxic Event from fossil wood and
777 marine carbonate (Lusitanian Basin, Portugal). Earth Planet. Sci. Lett. 253, 455–470.

778 Hites, R.A., Laflamme, R.E., Farrington, J.W., 1977. Sedimentary Polycyclic Aromatic
779 Hydrocarbons: The Historical Record. Science 198, 829–831.
780 Howarth, M., 1992. The ammonite family Hildoceratidae in the Lower Jurassic of
781 Britain. Palaeontogr. Soc. Monogr. 145, 1–106.
782 Jenkyns, H., 1988. The early Toarcian (Jurassic) anoxic event: stratigraphic, sedimentary,
783 and geochemical evidence. Am. J. Sci. 288, 101–151.
784 Jenkyns, H., Gröcke, D., Hesselbo, S., 2001. Nitrogen isotope evidence for water mass
785 denitrification during the early Toarcian (Jurassic) oceanic anoxic event.
786 Paleoceanography 16, 593–603.
787 Jenkyns, H.C., 1980. Cretaceous anoxic events: from continents to oceans. J. Geol. Soc.
788 (London) 137, 171–188.
789 Jenkyns, H.C., 2010. Geochemistry of oceanic anoxic events. Geochem. Geophys.
790 Geosyst. 11, Q03004.
791 Jiang, C., Alexander, R., Kagi, R.I., Murray, A.P., 1998. Polycyclic aromatic
792 hydrocarbons in ancient sediments and their relationships to palaeoclimate. Org.
793 Geochem. 29, 1721–1735.
794 Jiang, C., Alexander, R., Kagi, R.I., Murray, A.P., 2000. Origin of perylene in ancient
795 sediments and its geological significance. Org. Geochem. 31, 1545–1559.
796 Kawka, O.E., Simoneit, B.R.T., 1990. Polycyclic aromatic hydrocarbons in hydrothermal
797 petroleums from the Guaymas Basin spreading center. Appl. Geochem. 5, 17–27.
798 Kemp, D.B., Coe, A.L., Cohen, A.S., Schwark, L., 2005. Astronomical pacing of
799 methane release in the Early Jurassic period. Nature 437, 396–399.
800 Kemp, D.B., Coe, A.L., Cohen, A.S., Weedon, G.P., 2011. Astronomical forcing and
801 chronology of the early Toarcian (Early Jurassic) oceanic anoxic event in Yorkshire,
802 UK. Paleoceanography 26, PA4210.
803 Kiessling, W., Simpson, C., 2011. On the potential for ocean acidification to be a general
804 cause of ancient reef crises. Glob. Change Biol. 17, 56–67.
805 Killops, S.D., Massoud, M.S., 1992. Polycyclic aromatic hydrocarbons of pyrolytic
806 origin in ancient sediments: evidence for Jurassic vegetation fires. Org. Geochem. 18,
807 1–7.
808 Köster, J., van Kaam-Peters, H., Koopmans, M., de Leeuw, J., Sinninghe Damsté, J.,
809 1997. Sulphurisation of homohopanoids: Effects on carbon number distribution,
810 speciation, and 22S/22R epimer ratios. Geochim. Cosmochim. Acta 61, 2431–2452.
811 Kruge, M.A., Stankiewicz, B.A., Crelling, J.C., Montanari, A., Bensley, D.F., 1994.
812 Fossil charcoal in Cretaceous-Tertiary boundary strata: Evidence for catastrophic
813 firestorm and megawave. Geochim. Cosmochim. Acta 58, 1393–1397.
814 Kuypers, M.M.M., van Breugel, Y., Schouten, S., Erba, E., Sinninghe Damsté, J.S., 2004.
815 N_2-fixing cyanobacteria supplied nutrient N for Cretaceous oceanic anoxic events.
816 Geology 32, 853.
817 Lentz, S.J., Fewings, M.R., 2012. The Wind- and Wave-Driven Inner-Shelf Circulation.
818 Annu. Rev. Marine. Sci. 4, 317–343.
819 Luo, G., Wang, Y., Algeo, T.J., Kump, L.R., Bai, X., Yang, H., Yao, L., Xie, S., 2011.
820 Enhanced nitrogen fixation in the immediate aftermath of the latest Permian marine
821 mass extinction. Geology 39, 647–650.
822 Macquaker, J., Bentley, S.J., Bohacs, K.M., 2010. Wave-enhanced sediment-gravity
823 flows and mud dispersal across continental shelves: Reappraising sediment transport

processes operating in ancient mudstone successions. Geology 38, 947-950.
Macquaker, J., Taylor, K., 1996. A sequence stratigraphic interpretation of a mudstone-dominated succession: the Lower Jurassic Cleveland Ironstone Formation. J. Geol. Soc. (London) 153, 759–770.
Marynowski, L., Simoneit, B.R.T., 2009. Widespread Upper Triassic to Lower Jurassic wildfire records from Poland: Evidence from charcoal and pyrolytic polycyclic aromatic hydrocarbons. Palaios 24, 285–298.
McElwain, J.C., Wade-Murphy, J., Hesselbo, S.P., 2005. Changes in carbon dioxide during an oceanic anoxic event linked to intrusion into Gondwana coals. Nature 435, 479–482.
Meyer, K.M., Macalady, J.L., Fulton, J.M., Kump, L.R., Schaperdoth, I., Freeman, K.H., 2011. Carotenoid biomarkers as an imperfect reflection of the anoxygenic phototrophic community in meromictic Fayetteville Green Lake. Geobiol. 9, 321–329.
Moldowan, J.M., Sundararaman, P., Schoell, M., 1986. Sensitivity of biomarker properties to depositional environment and/or source input in the Lower Toarcian of SW-Germany. Org. Geochem. 10, 915–926.
Moldowan, J.M., Seifert, W.K., Gallegos, E.J., 1985. Relationship Between Petroleum Composition and Depositional Environment of Petroleum Source Rocks. Am. Assoc. Petr. Geol. B. 69, 1255–1268.
Naeher, S., Geraga, M., Papatheodorou, G., Ferentinos, G., Kaberi, H., Schubert, C. J., 2012. Environmental variations in a semi-enclosed embayment (Amvrakikos Gulf, Greece)- reconstructions based on benthic foraminifera abundance and lipid biomarker pattern. Biogeosciences 9, 5081-5094.
Naqvi, S., Naik, H., Pratihary, A., D'Souza, W., Narvekar, P., Jayakumar, D., Devol, A., Yoshinari, T., Saino, T., 2006. Coastal versus open-ocean denitrification in the Arabian Sea. Biogeosciences 3, 621–633.
Noble, R.A., Alexander, R., Kagi, R.I., Knox, J., 1986. Identification of some diterpenoid hydrocarbons in petroleum. Org. Geochem. 10, 825–829.
O'Brien, N., 1990. Significance of lamination in Toarcian (Lower Jurassic) shales from Yorkshire, Great Britain. Sediment. Geol. 67, 25–34.
Pálfy, J., Smith, P., 2000. Synchrony between Early Jurassic extinction, oceanic anoxic event, and the Karoo-Ferrar flood basalt volcanism. Geology 28, 747–750.
Pancost, R., Crawford, N., Magness, S., Turner, A., Jenkyns, H., Maxwell, J., 2004. Further evidence for the development of photic-zone euxinic conditions during Mesozoic oceanic anoxic events. J. Geol. Soc. (London) 161, 353–364.
Pancost, R., Freeman, K., Patzkowsky, M., 1999. Organic-matter source variation and the expression of a late Middle Ordovician carbon isotope excursion. Geology 27, 1015–1018.
Peters, K.E., Walters, C.C., Moldowan, J.M., 2005. The Biomarker Guide: Biomarkers and Isotopes In Petroleum Systems and Earth History, 2nd ed, The Biomarker Guide: Biomarkers and Isotopes in Petroleum Systems and Earth History. Cambridge University Press.
Powell, J.H., 2010. Jurassic sedimentation in the Cleveland Basin: a review. Proc. Yorks. Geol. Soc. 58, 21–72.
Prauss, M., Ligouis, B., Luterbacher, H., 1991. Organic matter and palynomorphs in the

870 "Posidonienschiefer" (Toarcian, Lower Jurassic) of southern Germany. Geol. Soc.,
871 London Spec. Publ. 58, 335–351.
872 Rashby, S., Sessions, A.L., Summons, R.E., Newman, D., 2007. Biosynthesis of 2-
873 methylbacteriohopanepolyols by an anoxygenic phototroph. Proc. Natl. Acad. Sci.
874 U.S.A 104, 15099.
875 Röhl, H., Schmid, A., Oschmann, W., Frimmel, A., Schwark, L., 2001. The Posidonia
876 Shale (Lower Toarcian) of SW-Germany: an oxygen-depleted ecosystem controlled
877 by sea level and palaeoclimate. Palaeogeogr. Palaeoclimatol. Palaeoecol. 165, 27–52.
878 Sabatino, N., Neri, R., Bellanca, A., Jenkyns, H.C., Baudin, F., Parisi, G., Masetti, D.,
879 2009. Carbon-isotope records of the Early Jurassic (Toarcian) oceanic anoxic event
880 from the Valdorbia (Umbria-Marche Apennines) and Monte Mangart (Julian Alps)
881 sections: palaeoceanographic and stratigraphic implications. Sedimentology 56,
882 1307–1328.
883 Sãenz, J.P., Eglinton, T.I., Summons, R.E., 2011. Abundance and structural diversity of
884 bacteriohopanepolyols in suspended particulate matter along a river to ocean transect.
885 Org. Geochem. 42, 774–780.
886 Schlanger, S.O., Jenkyns, H.C., 1976. Cretaceous oceanic anoxic events: causes and
887 consequences. Geol. Mijnbouw 55, 179–184.
888 Schouten, S., van Kaam-Peters, H., Rijpstra, W., Schoell, M., Sinninghe Damsté , J.,
889 2000. Effects of an oceanic anoxic event on the stable carbon isotopic composition of
890 Early Toarcian carbon. Am. J. Sci. 300, 1–22.
891 Schouten, S., Woltering, M., Rijpstra, W.I.C., Sluijs, A., Brinkhuis, H., Sinninghe
892 Damsté, J.S., 2007. The Paleocene–Eocene carbon isotope excursion in higher plant
893 organic matter: Differential fractionation of angiosperms and conifers in the Arctic.
894 Earth Planet. Sci. Lett. 258, 581–592.
895 Schunck, H., Lavik, G., Desai, D.K., Großkopf, T., Kalvelage, T., Löscher, C.R.,
896 Paulmier, A., Contreras, S., Siegel, H., Holtappels, M., Rosenstiel, P., Schilhabel,
897 M.B., Graco, M., Schmitz, R.A., Kuypers, M.M.M., LaRoche, J., 2013. Giant
898 Hydrogen Sulfide Plume in the Oxygen Minimum Zone off Peru Supports
899 Chemolithoautotrophy. PLoS One 8, e68661.
900 Schwark, L., Frimmel, A., 2004. Chemostratigraphy of the Posidonia Black Shale, SW-
901 Germany. Chem. Geol. 206, 231–248.
902 Sephton, M.A., Love, G.D., Meredith, W., Snape, C.E., Sun, C.-G., Watson, J.S., 2005.
903 Hydropyrolysis: A new technique for the analysis of macromolecular material in
904 meteorites. Planet. Space Sci. 53, 1280–1286.
905 Sepúlveda, J., Wendler, J., Leider, A., Kuss, H–J., Summons, R.E., Hinrichs, K–U., 2009.
906 Molecular isotopic evidence of environmental and ecological changes across the
907 Cenomanian–Turonian boundary in the Levant Platform of central Jordan. Org.
908 Geochem. 40, 553–568.
909 Sinninghe Damsté, J.S., Schouten, S., Biological markers for anoxia in the photic zone of
910 the water column. In: The Handbook of Environmental Chemistry, (Springer-Verlag,
911 Berlin), pp. 127–163.
912 Sinninghe Damsté, J., Kenig, F., Koopmans, M., Köster, J., Schouten, S., Hayes, J., de
913 Leeuw, J., 1995. Evidence for gammacerane as an indicator of water column
914 stratification. Geochim. Cosmochim. Acta 59, 1895–1900.
915 Smith, F., Wing, S., Freeman, K., 2007. Magnitude of the carbon isotope excursion at the

916 Paleocene–Eocene thermal maximum: The role of plant community change. Earth
917 Planet. Sci. Lett. 262, 50–65.
918 Smittenberg, R.H., Pancost, R.D., Hopmans, E.C., Paetzel, M., and Sinninghe Damsté,
919 J.S., 2004, A 400-year record of environmental change in an euxinic fjord as revealed
920 by the sedimentary biomarker record: Palaeogeogr. Palaeoclimatol. Palaeoecol. 202,
921 331–351.
922 Stewart, F.J., Ulloa, O., DeLong, E.F., 2012. Microbial metatranscriptomics in a
923 permanent marine oxygen minimum zone. Environ. Microbiol. 14, 23–40.
924 Suan, G., Nikitenko, B.L., Rogov, M.A., Baudin, F., Spangenberg, J.E., Knyazev, V.G.,
925 Glinskikh, L.A., Goryacheva, A.A., Adatte, T., Riding, J.B., Föllmi, K.B., Pittet, B.,
926 Mattioli, E., Lécuyer, C., 2011. Polar record of Early Jurassic massive carbon
927 injection. Earth Planet. Sci. Lett. 312, 102–113.
928 Suan, G., Pittet, B., Bour, I., Mattioli, E., Duarte, L., Mailliot, S., 2008. Duration of the
929 Early Toarcian carbon isotope excursion deduced from spectral analysis:
930 Consequence for its possible causes. Earth Planet. Sci. Lett. 267, 666–679.
931 Summons, R.E., Jahnke, L., Hope, J., Logan, G., 1999. 2-Methylhopanoids as biomarkers
932 for cyanobacterial oxygenic photosynthesis. Nature 23, 85–88.
933 Talbot, H., Farrimond, P., 2007. Bacterial populations recorded in diverse sedimentary
934 biohopanoid distributions. Org. Geochem. 38, 1212–1225.
935 Talbot, H.M., Watson, D.F., Pearson, E.J., Farrimond, P., 2003. Diverse biohopanoid
936 compositions of non-marine sediments. Org. Geochem. 34, 1353–1371.
937 Talbot, M., Livingstone, D., 1989. Hydrogen Index and Carbon Isotopes of Lacustrine
938 Organic-Matter as Lake Level Indicators. Palaeogeogr. Palaeoclimatol. Palaeoecol.
939 70, 121–137.
940 Tang, Y., Huang, Y., Ellis, G.S., Wang, Y., Kralert, P.G., Gillaizeau, B., Ma, Q., Hwang,
941 R., 2005. A kinetic model for thermally induced hydrogen and carbon isotope
942 fractionation of individual n-alkanes in crude oil. Geochim. Cosmochim. Acta 69,
943 4505–4520.
944 ten Haven, H., Rohmer, M., Rullkötter, J., Bisseret, P., 1989. Tetrahymanol, the most
945 likely precursor of gammacerane, occurs ubiquitously in marine sediments. Geochim.
946 Cosmochim. Acta 53, 3073–3079.
947 Trabucho-Alexandre, J., Dirkx, R., Veld, H., Klaver, G., de Boer, P., 2012. Toarcian
948 Black Shales in the Dutch Central Graben: Record of Energetic, Variable
949 Depositional Conditions during an Oceanic Anoxic Event. J. Sediment. Res. 82, 104-
950 120.
951 Trabucho-Alexandre, J., Tuenter, E., Henstra, G., van der Zwan, K., van de Wal, R.,
952 Dijkstra, H., de Boer, P., 2010. The mid-Cretaceous North Atlantic nutrient trap:
953 Black shales and OAEs. Paleoceanography 25, PA4201.
954 van Breugel, Y., Baas, M., Schouten, S., Mattioli, E., Sinninghe Damsté, J.S., 2006.
955 Isorenieratane record in black shales from the Paris Basin, France: Constraints on
956 recycling of respired CO_2 as a mechanism for negative carbon isotope shifts during
957 the Toarcian oceanic anoxic event. Paleoceanography 21, PA4220.
958 van de Schootbrugge, B., McArthur, J.M., Bailey, T.R., Rosenthal, Y., Wright, J.D.,
959 Miller, K.G., 2005. Toarcian oceanic anoxic event: An assessment of global causes
960 using belemnite C isotope records. Paleoceanography 20, PA3008.
961 Venkatesan, M.I., Dahl, J., 1989. Organic geochemical evidence for global fires at the

962 Cretaceous/Tertiary boundary. Nature 338, 57–60.
963 Vetö, I., Demeny, A., Hertelendi, E., Hetenyi, M., 1997. Estimation of primary
964 productivity in the Toarcia Tethys- a novel approach based on TOC, reduced sulphur
965 and manganese contents. Palaeogeogr. Palaeoclimatol. Palaeoecol. 132, 355–371.
966 Wahlund, T., Woese, C., Castenholz, R., Madigan, M., 1991. A thermophilic green sulfur
967 bacterium from New Zealand hot springs, *Chlorobium tepidum* sp. nov. Arch.
968 Microbiol. 156, 81–90.
969 Wakeham, S., Schaffner, C., Giger, W., 1980. Polycyclic aromatic hydrocarbons in
970 Recent lake sediments--I. Compounds having anthropogenic origins. Geochim.
971 Cosmochim. Acta 44, 403–413.
972 Wakeham, S.G., Amann, R., Freeman, K.H., Hopmans, E.C., Jørgensen, B.B., Putnam,
973 I.F., Schouten, S., Sinninghe Damsté, J.S., Talbot, H.M., Woebken, D., 2007.
974 Microbial ecology of the stratified water column of the Black Sea as revealed by a
975 comprehensive biomarker study. Org. Geochem. 38, 2070–2097.
976 Wakeham, S.G., Turich, C., Schubotz, F., Podlaska, A., Li, X., Varela, R., Astor, Y.,
977 Sãenz, J.P, Rush, D., Sinninghe Damsté , J.S., Summons, R.E., Scranton, M.I.,
978 Taylor, G. T., Hinrichs, K.-U., 2012. Biomarkers, chemistry, and microbiology show
979 chemoautotrophy in a multilayer chemocline in the Cariaco Basin. Deep-Sea Res. I
980 163, 133-156.
981 Wen, Z., Ruiyong, W., Radke, M., Qingyu, W., Guoying, S., Zhili, L., 2000. Retene in
982 pyrolysates of algal and bacterial organic matter. Org. Geochem. 31, 757–762.
983 Wignall, P., Newton, R.J., Little, C.T.S., 2005. The timing of paleoenvironmental change
984 and cause-and-effect relationships during the Early Jurassic mass extinction in
985 Europe. Am. J. Sci. 305, 1014–1032.
986 Xie, S., Pancost, R., Yin, H., Wang, H., Evershed, R., 2005. Two episodes of microbial
987 change coupled with Permo/Triassic faunal mass extinction. Nature 434, 494–497.
988 Zhang, C., Zhang, Y., Cai, C., 2011. Aromatic isoprenoids from the 25-65 Ma saline
989 lacustrine formations in the western Qaidam Basin, NW China. Org. Geochem. 42,
990 851-855.
991 Zundel, M., Rohmer, M., 1985. Prokaryotic triterpenoids. 1. 3β-Methylhopanoids from
992 *Acetobacter* species and *Methylococcus capsulatus*. Eur. J. Biochem. 150, 23–27.
993

Figure 1

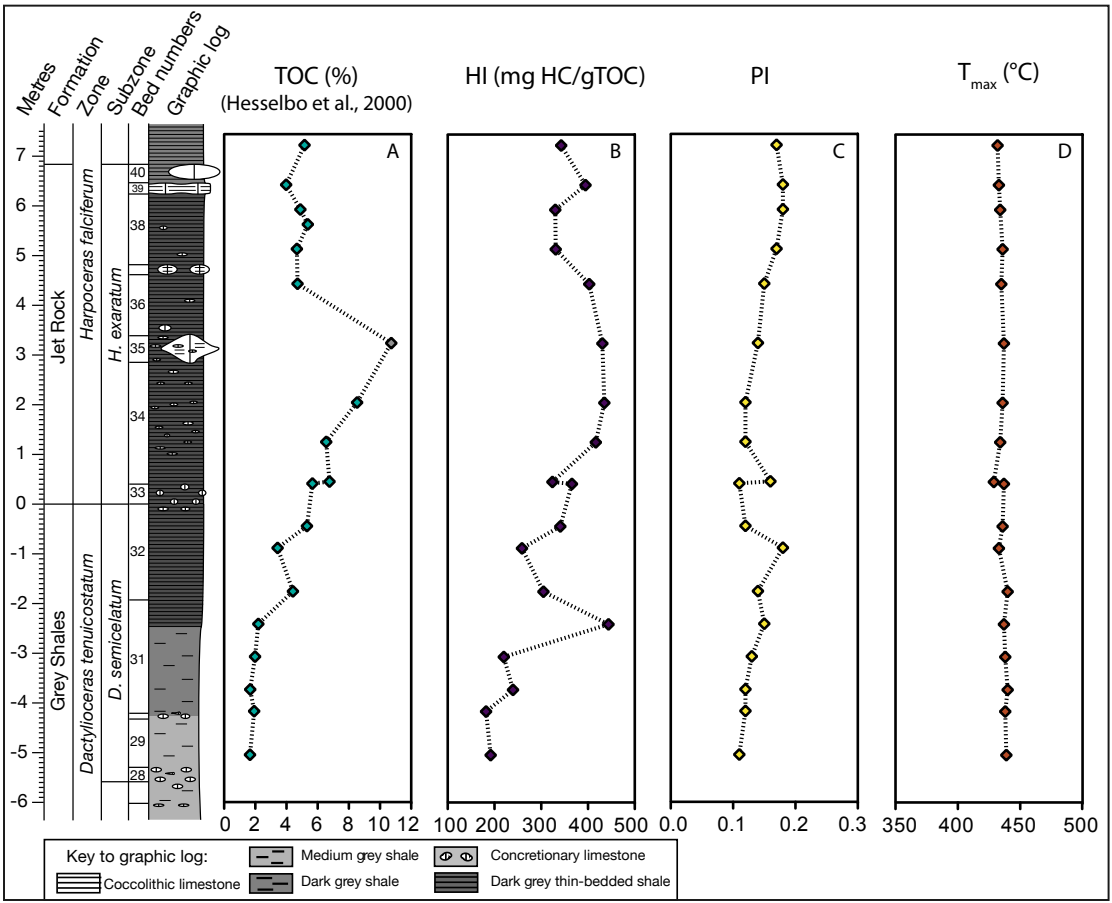
Metres
Formation
Zone
Subzone
Bed numbers
Graphic log
Jet Rock
Grey Shales
Harpoceras falciferum
H. exaratum
Dactylioceras tenuicostatum
D. semicelatum
TOC (%)
(Hesselbo et al., 2000)
HI (mg HC/gTOC)
PI
T max (°C)
A
B
C
D
Key to graphic log:
Coccolithic limestone
Medium grey shale
Dark grey shale
Concretionary limestone
Dark grey thin-bedded shale

Figure 2

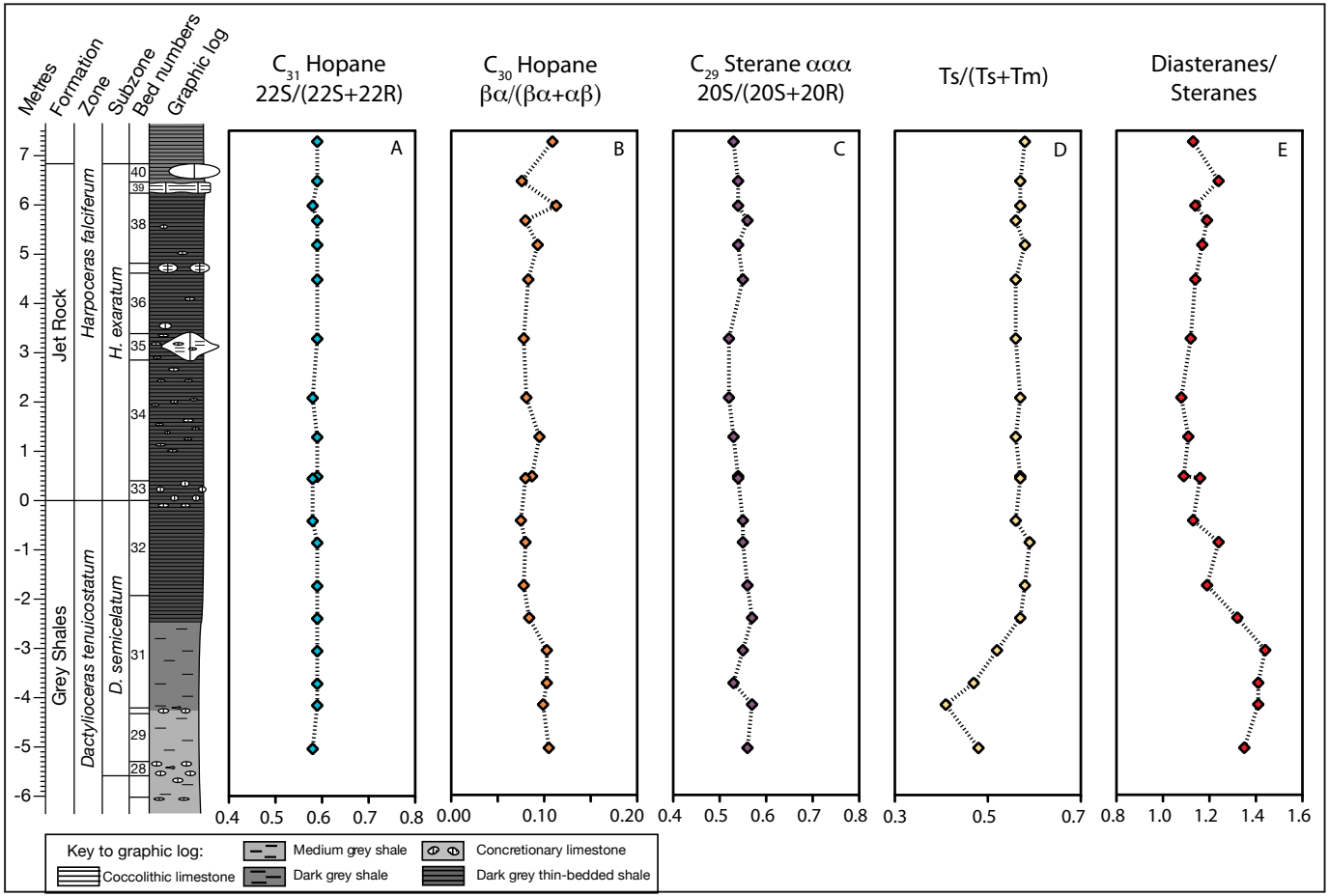
Metres
Formation
Zone
Subzone
Bed numbers
Graphic log
Jet Rock
Grey Shales
Harpoceras falciferum
H. exaratum
Dactylioceras tenuicostatum
D. semicelatum
40
39
38
36
35
34
33
32
31
29
28
7
6
5
4
3
2
1
0
-1
-2
-3
-4
-5
-6
C31 Hopane
22S/(22S+22R)
A
0.4
0.5
0.6
0.7
0.8
C30 Hopane
βα/(βα+αβ)
B
0.00
0.10
0.20
C29 Sterane ααα
20S/(20S+20R)
C
0.4
0.5
0.6
0.7
0.8
Ts/(Ts+Tm)
D
0.3
0.5
0.7
Diasteranes/
Steranes
E
0.8
1.0
1.2
1.4
1.6
Key to graphic log:
Coccolithic limestone
Medium grey shale
Dark grey shale
Concretionary limestone
Dark grey thin-bedded shale

Figure 3

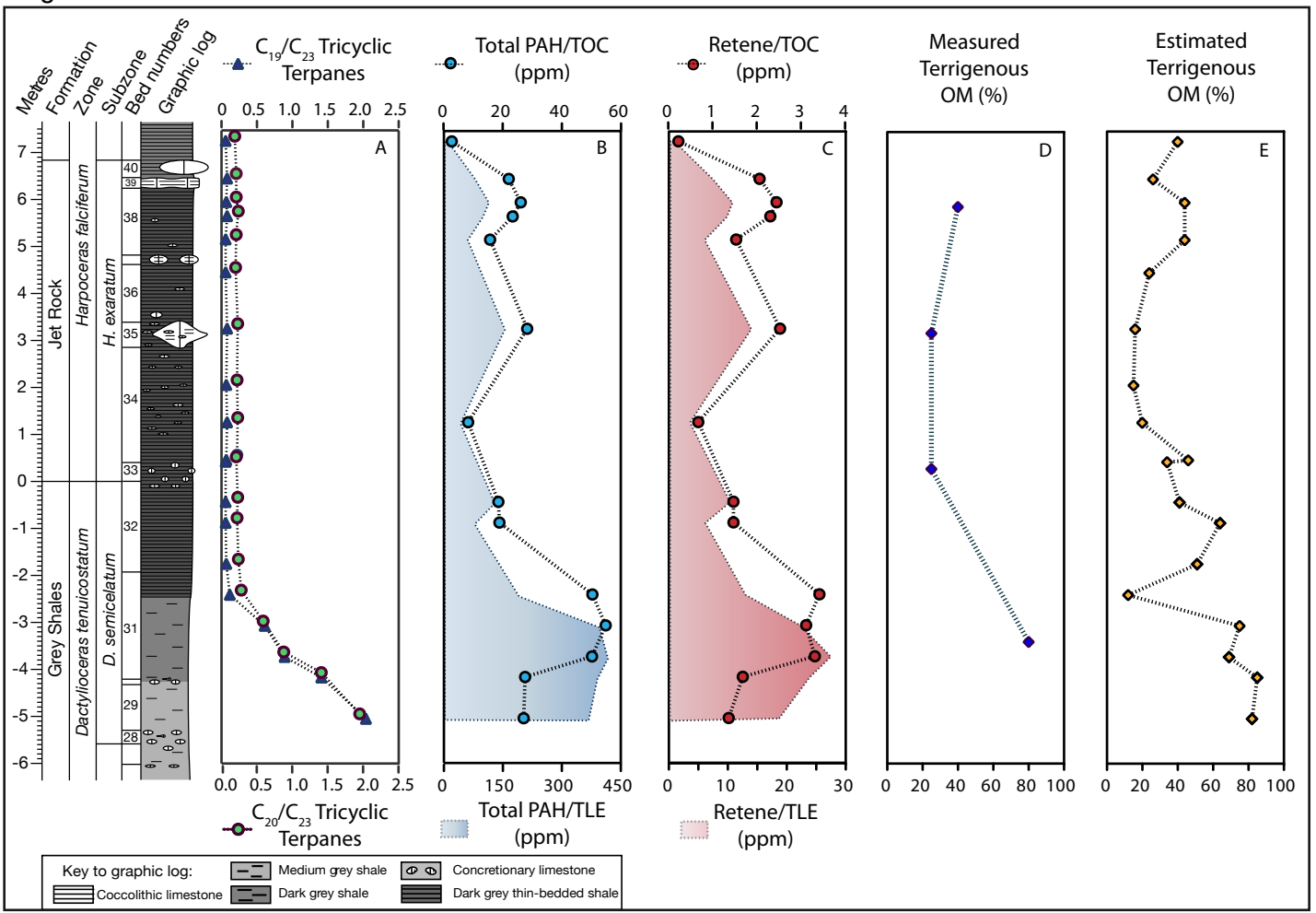
Metres
Formation
Zone
Subzone
Bed numbers
Graphic log
Jet Rock
Grey Shales
Harpoceras falciferum
H. exaratum
D. semicelatum
Dactylioceras tenuicostatum
C19/C23 Tricyclic Terpanes
C20/C23 Tricyclic Terpanes
Total PAH/TOC (ppm)
Total PAH/TLE (ppm)
Retene/TOC (ppm)
Retene/TLE (ppm)
Measured Terrigenous OM (%)
Estimated Terrigenous OM (%)
A
B
C
D
E
Key to graphic log:
Coccolithic limestone
Medium grey shale
Dark grey shale
Concretionary limestone
Dark grey thin-bedded shale

Figure 4

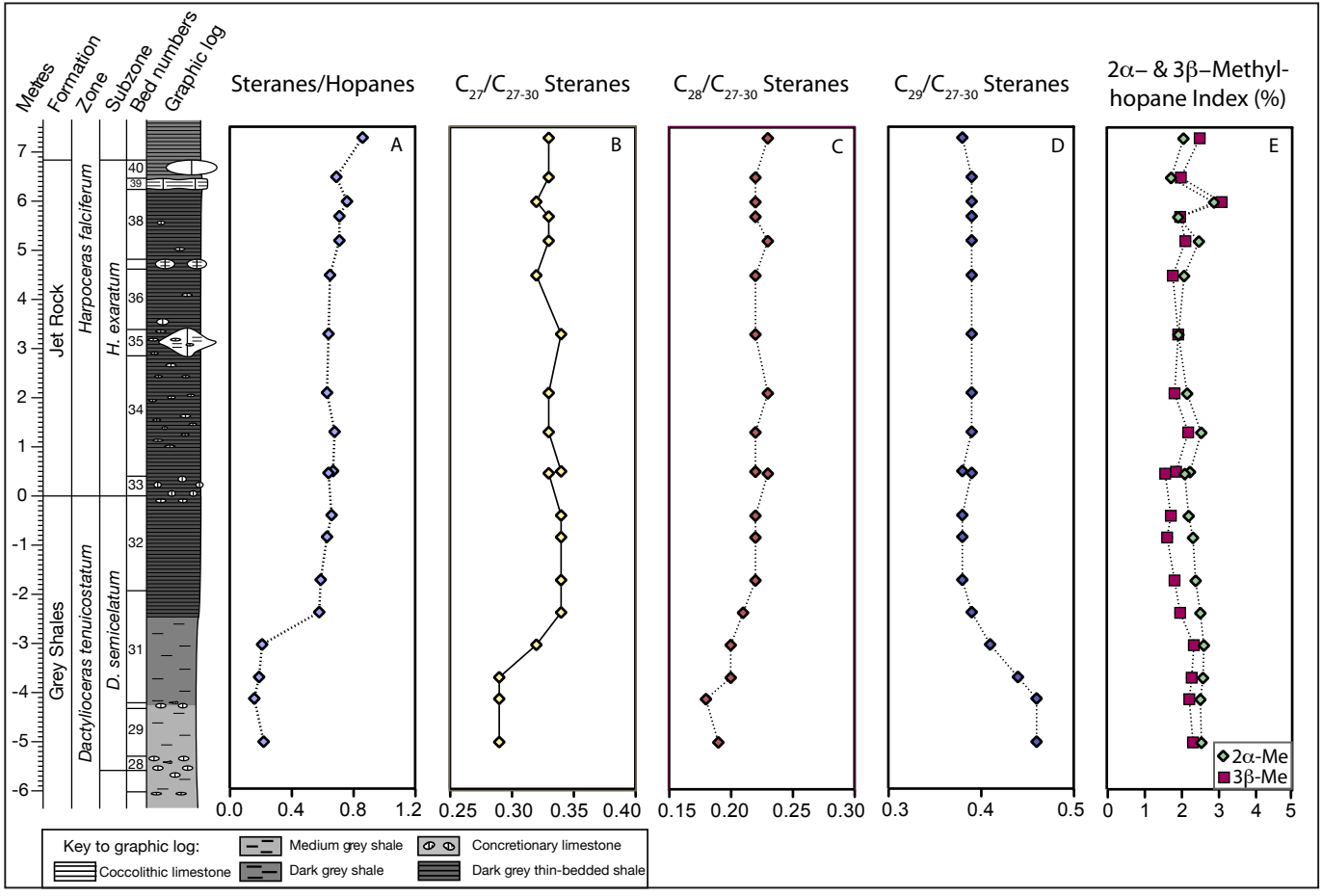
Metres
Formation
Zone
Subzone
Bed numbers
Graphic log
Jet Rock
Grey Shales
Harpoceras falciferum
Dactylioceras tenuicostatum
H. exaratum
D. semicelatum
40
39
38
36
35
34
33
32
31
29
28
Steranes/Hopanes
A
0.0 0.4 0.8 1.2
C27/C27-30 Steranes
B
0.25 0.30 0.35 0.40
C28/C27-30 Steranes
C
0.15 0.20 0.25 0.30
C29/C27-30 Steranes
D
0.3 0.4 0.5
2α– & 3β–Methyl-hopane Index (%)
E
0 1 2 3 4 5
2α-Me
3β-Me
Key to graphic log:
Coccolithic limestone
Medium grey shale
Dark grey shale
Concretionary limestone
Dark grey thin-bedded shale

Figure 5

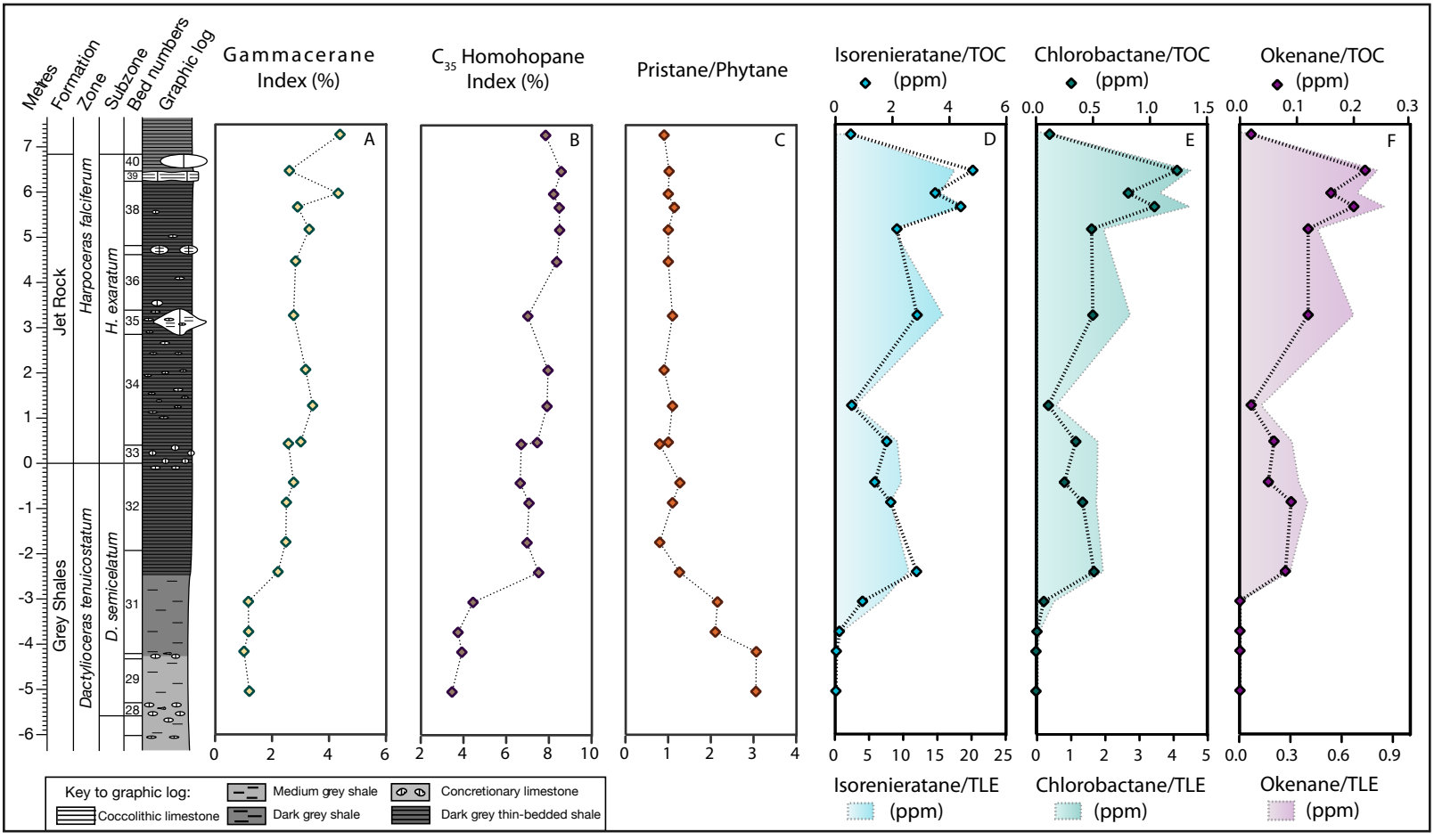
Metres
Formation
Zone
Subzone
Bed numbers
Graphic log
Jet Rock
Grey Shales
Harpoceras falciferum
Dactylioceras tenuicostatum
H. exaratum
D. semicelatum
Gammacerane Index (%)
A
C35 Homohopane Index (%)
B
Pristane/Phytane
C
Isorenieratane/TOC (ppm)
D
Chlorobactane/TOC (ppm)
E
Okenane/TOC (ppm)
F
Isorenieratane/TLE (ppm)
Chlorobactane/TLE (ppm)
Okenane/TLE (ppm)
Key to graphic log:
Coccolithic limestone
Medium grey shale
Dark grey shale
Concretionary limestone
Dark grey thin-bedded shale

Figure 6

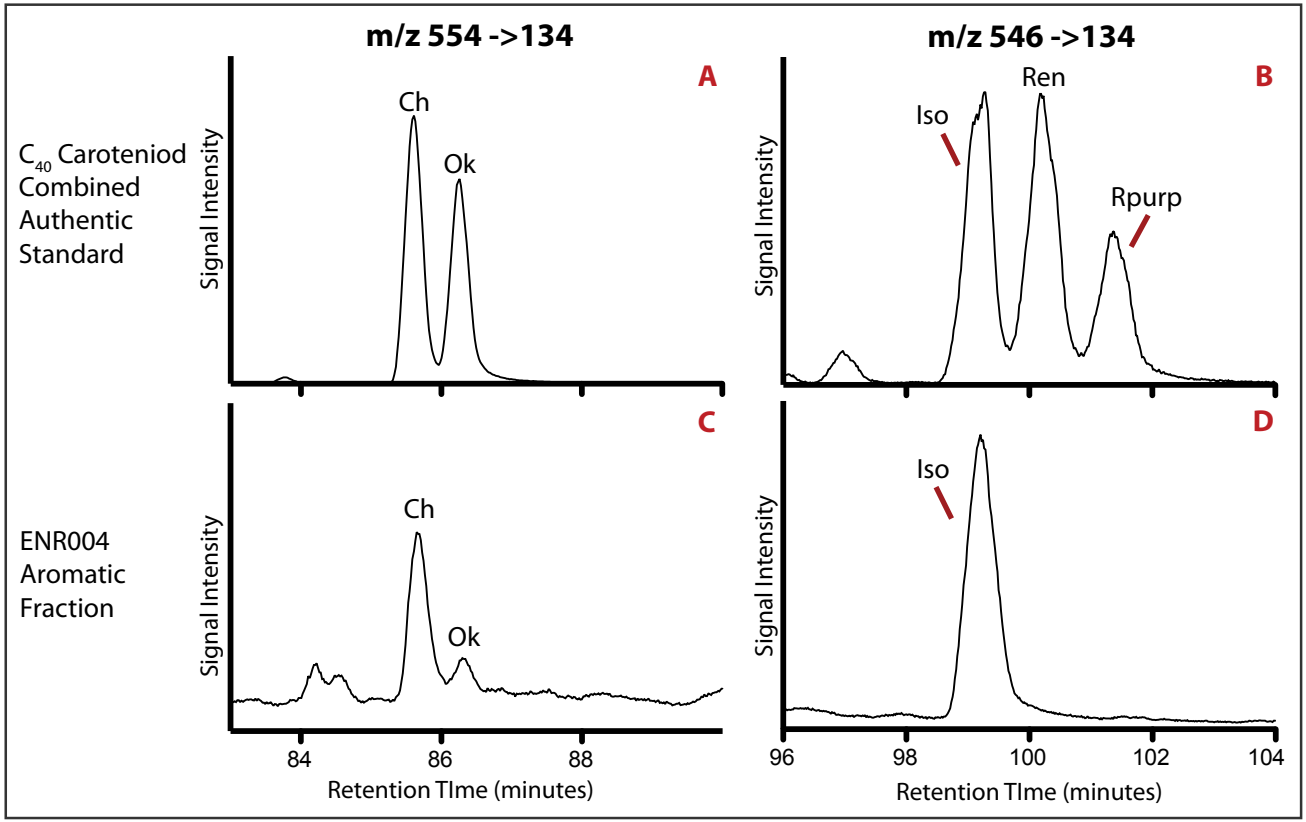
m/z 554 ->134
m/z 546 ->134
A
B
C
D
C_{40} Carotenoid Combined Authentic Standard
ENR004 Aromatic Fraction
Signal Intensity
Ch
Ok
Iso
Ren
Rpurp
84
86
88
96
98
100
102
104
Retention TIme (minutes)

Figure 7

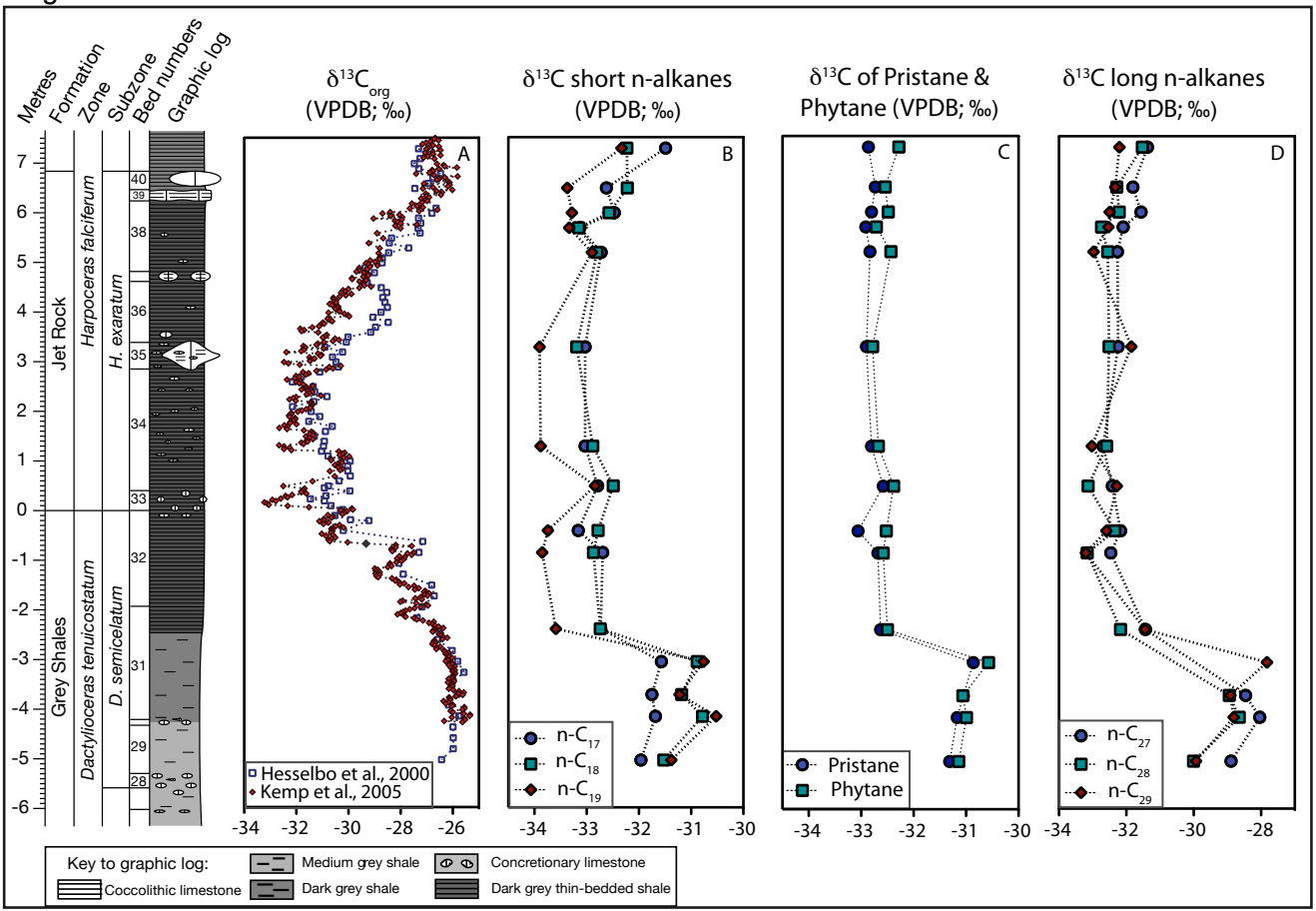
Metres
Formation
Zone
Subzone
Bed numbers
Graphic log
Jet Rock
Grey Shales
Harpoceras falciferum
Dactylioceras tenuicostatum
H. exaratum
D. semicelatum
δ13Corg (VPDB; ‰)
A
Hesselbo et al., 2000
Kemp et al., 2005
δ13C short n-alkanes (VPDB; ‰)
B
n-C17
n-C18
n-C19
δ13C of Pristane & Phytane (VPDB; ‰)
C
Pristane
Phytane
δ13C long n-alkanes (VPDB; ‰)
D
n-C27
n-C28
n-C29
Key to graphic log:
Coccolithic limestone
Medium grey shale
Dark grey shale
Concretionary limestone
Dark grey thin-bedded shale

Supplementary Online Material (SOM)

3.1 Rock-Eval pyrolysis

Powdered sediment samples (~1 g) were analyzed at the University of Newcastle on a Rock-Eval pyrolysis instrument. The total organic carbon (TOC %), T_{max} (°C), S_1, and S_2 were determined. The S_1 and S_2 are expressed in mg hydrocarbons (HC) per gram dry rock. These parameters were used to calculate the hydrogen index (HI) (HI=[100*S_2]/TOC; expressed in mg hydrocarbon (HC)/g TOC) and the production index (PI) (PI= S_1/[S_1+S_2]). The Rock-Eval TOC values and the bulk $\delta^{13}C_{org}$ have been previously reported (Hesselbo et al., 2000).

3.2 Organic petrography

In order to examine the nature of the organic matter, particularly the fraction of terrigenous organic matter, four samples across the section were prepared for optical analysis of the kerogen. Kerogen was isolated from the sample material remaining after lipid extraction as described in section 3.3. The mineral matrix was removed by the sequential addition of HCl and HF. Samples were centrifuged and rinsed between acid treatments, and the residual matter was rinsed with water and methanol. A subsample of each kerogen sample was mounted onto a slide in duplicate and assessed optically under white light and fluorescent light using a Zeiss research microscope and a Zeiss x 40 Plan-Neofluar objective. A Zeiss Axioskop, Axio Image D1, and a Zeiss 18 filter set were used to take photomicrographs and fluorescence images.

The fraction of terrigenous organic matter was estimated for the samples that were not analyzed by organic petrography using the linear relationship between the percent terrigenous organic matter measured by optical microscopy and the corresponding HI:

$$f_{Terr\ OM}\ (\%) = -0.279 * HI + 136 \quad (1)$$

where the linear regression had an R^2 value of 0.90 and $f_{Terr\ OM}$ represents the terrigenous organic matter as a percentage.

3.3 Biomarker extraction and analysis

Powdered samples (~ 5 g) were extracted using a Dionex ASE 200 Accelerated Solvent Extractor at 1000 psi and 100°C, with a solvent mixture of dichloromethane:methanol 9:1 (v/v). The total lipid extract (TLE) was reacted with acid-activated copper shots to remove elemental sulfur. Asphaltenes were separated (3x) from the maltene fraction by precipitation in n-pentane at 4ºC, and after centrifugation at 3000 rpm for 10 minutes. The maltene fraction was then separated into saturated, aromatic, and polar fractions by silica gel chromatography using hexane, 1:1 (v/v) hexane/dichloromethane, and 7:3 (v/v) dichloromethane/methanol.

The saturated fractions were screened by gas chromatography-mass spectrometry (GC-MS) in full scan using an Agilent 6890 GC equipped with a HP6890 autosampler and interfaced to an Agilent 5973 mass spectrometer. Saturated hydrocarbons were also analyzed by gas chromatography-metastable reaction monitoring-mass spectrometry (GC-MRM-MS) on a Micromass Autospec Ultima mass spectrometer coupled with an Agilent 6890N GC. The analysis was carried out with a 60 m J&W Scientific DB-1 fused silica capillary column (internal diameter: 0.25 mm; 0.25 m film thickness) in pulsed splitless mode. The initial GC oven temperature was programmed to 60°C (held for 2

minutes), ramped to 150°C at 10°C/minute, and then to 315°C at 3°C/minute (held for 24 minutes). The ion source was in EI mode at a temperature of 250°C, an ionization energy of 70 eV, and acceleration voltage of 8000 kV. Tricyclic terpanes and hopanes were identified by MRM using the molecular ion to the m/z 191 transitions. Likewise, steranes were identified by MRM using the molecular ion to m/z 217 transitions.

The aromatic fraction was analyzed by GC-MS in SIM modes. Prior to analysis, 400 ng of an aromatic internal standard, deuterated phenanthrene, was added to each sample. The GC was fitted with a DB-5 stationary phase column, and the GC oven temperature was ramped from 60°C to 150°C at 20°C/minute, and then to 330°C at 4°C/minute (held for 27 minutes). The aryl isoprenoids and isorenieratane was identified in the m/z 134 ion chromatograms and quantified using the internal standard. Absolute quantification is not possible without taking into account relative response factors but our approach does allow an internally consistent estimation across the sample set.

The aromatic fraction was also analyzed by GC-MS in full scan and MRM modes on a Micromass Autospec Ultima mass spectrometer coupled with an Agilent 6890N GC autospec. The GC was fitted with a DB-5 stationary phase column. Polycyclic aromatic hydrocarbons (PAHs) were identified and quantified in full scan mode by their mass spectra and by comparison with a mix of authentic standards, with the exception of retene, coronene, and triphenylene, which were identified by their mass spectra and relative retention time. Aromatic carotenoid derivatives were also analyzed by GC-MRM-MS using parent-daughter reactions. Isorenieratane, okenane, and chlorobactane were identified in characteristic MRM transitions by comparison of retention times to an extract from the Barney Creek Formation (BCF) and a standard mix of hydrogenated

carotenoids containing chlorobactane, okenane, isorenieratane, renieratane, and renierapurpane. Using the MRM data, okenane and chlorobactane were quantified against the GC-MSD quantified isorenieratane. The aromatic carotenoid derivative and PAH concentrations were normalized against mass of TLE and TOC.

Compound specific carbon isotopic measurements of saturated hydrocarbons were made by gas chromatography/combustion/ isotope ratio mass spectrometry (GC-C-IRMS) using a Thermo Finnigan Delta plus XP coupled to a Thermo Finnigan Trace GC. The initial oven temperature was programmed to 60°C (held for 3 minutes), ramped to 180°C at 10°C/min, and then to 320°C at 4°C/min (held for 20 minutes). All samples were bracketed by pulses of in house calibrated reference CO_2 gas and Oztech calibrated reference CO_2 gas. A standard mix of *n*-alkanes (mix A; Arndt Schimmelmann, Indiana University) was analyzed twice a day to monitor the instrument condition. The mean value of triplicate analyses are reported here in permil (‰) relative to Vienna Pee Dee belemnite (VPDB), and the standard deviation from the mean value was better than 0.4‰.